Contrib Mineral Petrol (2015) 169:45
DOI 10.1007/s00410-015-1128-5

ORIGINAL PAPER

Experimental determination of trace element partition coefficients between spinel and silicate melt: the influence of chemical composition and oxygen fugacity

C. H. Wijbrans[1,2] · S. Klemme[1] · J. Berndt[1] · C. Vollmer[1]

Received: 29 August 2014 / Accepted: 5 March 2015 / Published online: 23 April 2015

Abstract We present new experimentally determined trace element partition coefficients between spinel and silicate melt. The experiments were performed at atmospheric pressure and at temperatures between 1220 and 1450 °C. To study the effect of redox conditions on trace element partitioning, we performed experiments under different redox conditions, with fO_2 ranging from log −12 to log −0.7. The effect of different spinel compositions is also investigated. Our results show that spinel of all compositions readily incorporates the transition metals Ni, Co and Ga and the corresponding partition coefficients are >1. $D_{Ni,Co,Ga}$ are not significantly affected by changing melt composition, crystal composition or redox conditions. However, the multivalent trace elements V and Mo show a strong effect of redox conditions on their partitioning behavior with D_V and D_{Mo} highest at very reducing conditions and considerably lower at more oxidizing conditions. Partition coefficients for the high field strength elements Ti, Zr, Hf, Nb, and Ta and the elements Sc and Lu strongly depend on crystal composition, with D_{Ti} and D_{Sc} >1 for very Fe^{3+}- or Cr-rich (and Al-poor) spinels, but one to two orders of magnitude lower in systems with Al-rich spinels. We present some examples on how our data may be used to reconstruct redox conditions of spinel formation. We also present some results on the partitioning of Pt and Rh between spinel and melt. D_{Rh} depends strongly on redox conditions, while D_{Pt} is not significantly affected.

Keywords Spinel · Partition coefficients · Oxygen fugacity · Transition metals · High field strength elements · Platinum group elements

Communicated by Mark S Ghiorso.

Electronic supplementary material The online version of this article (doi:10.1007/s00410-015-1128-5) contains supplementary material, which is available to authorized users.

✉ C. H. Wijbrans
clazina.wijbrans@erdw.ethz.ch

[1] Institut für Mineralogie, Westfälische Wilhelms Universität Münster, Corrensstrasse 24, 48149 Münster, Germany

[2] Present Address: Institute of Geochemistry and Petrology, ETH Zürich, Clausiusstrasse 25, 8092 Zürich, Switzerland

Introduction

Spinel-structured oxides are common accessory minerals that occur in a variety of rocks such as evolved basaltic magmas, ultramafic rocks and metamorphic or sedimentary rocks (Arai 1992; Dick and Bullen 1984; Roeder and Reynolds 1991). Spinel can be a host mineral for a number of trace elements, most notably the transition metals, as well as HFSEs (high field strength elements; Nb, Ta, Zr and Hf) (Nielsen et al. 1994). Although spinel is typically only a minor component in most rocks, high partition coefficients for these elements mean that it might play an important role in the trace element budget of igneous rocks, and spinel trace element chemistry can be an important tool to determine fractionation trends or origins of magmas. Furthermore, (Cr)-spinel is associated with economically important platinum group element (PGE) deposits (see for example Ballhaus and Sylvester 2000; Naldrett et al. 2009). In order to understand the behavior of trace elements in magmatic systems, one needs a full set of experimentally determined partition coefficients. Currently, however, the available dataset is far from complete.

Trace element partitioning may depend on a number of factors including temperature, pressure and the chemical

composition of the crystal and melt (Blundy and Wood 1994). Different redox conditions may also play a role for multivalent elements. Furthermore, in the case of spinel, the crystallization of spinel itself depends on oxygen fugacity (Hill and Roeder 1974). For major magmatic mineral phases such as pyroxenes and garnet, experimental datasets as well as predictive models for element partitioning are available (Blundy and Wood 2003; van Westrenen and Draper 2007). For accessory phases, however, experimental data are not very abundant. Spinel partition coefficients have been determined experimentally in a few recent and older studies, many focusing on PGE partitioning (Brenan et al. 2012; Capobianco and Drake 1990; Capobianco et al. 1994; Righter et al. 2004; Sattari et al. 2002), while others report partitioning data for transition metals and/or HFSEs (Davis et al. 2013; Horn et al. 1994; Nielsen and Beard 2000; Nielsen et al. 1994; Righter et al. 2006).

Determining the partition coefficients of transition metals is complicated due to the fact that these elements often have multiple valence states, and partitioning may therefore be dependent on redox conditions. For natural spinel type oxides, several endmember compositions exist that exhibit complex solid solutions. In magmatic rocks, the most important endmembers that occur are spinel senso stricto ($MgAl_2O_4$), (magnesio-)chromite ((Fe^{2+}, Mg)Cr_2O_4) and magnetite ($Fe^{2+}Fe_2{}^{3+}O_4$) (Barnes and Roeder 2001). It may be expected that the major element composition of spinel has an effect on the partitioning behavior of trace elements. This has already been shown to be the case for (Ti-)magnetite-rich spinels by Nielsen et al. (1994) and Nielsen and Beard (2000), but the data are scarce for Al-rich spinel and chromite. Because of the difference in crystallographic structure between the mainly inversely structured magnetite and the mainly normal Cr or Al-spinel, it cannot be assumed that trace element partitioning of Al-spinel or chromite is similar to that of spinel with a high magnetite component.

To address these issues, we determined the partitioning of trace elements between spinels of different compositions and silicate melts, focusing mainly on Al- and Cr-rich spinels. To investigate the effect of different redox conditions on the partitioning of trace elements, we conducted experiments at a range of different oxygen fugacities.

Methods

Starting materials

The initial starting composition was selected from a phase diagram in the system $CaO–MgO–Al_2O_3–SiO_2$ (Yang et al. 1972), to ensure that spinel is the liquidus phase at 1300 °C. Further, starting compositions were modified from this initial mixture by replacing MgO by FeO, or Al_2O_3 by Cr_2O_3. The compositions of all starting materials are listed in Table 1. Starting materials were synthesized from oxides and carbonates (SiO_2, TiO_2, $CaCO_3$, MgO, Al_2O_3 and Fe_2O_3). MgO was fired at 1000 °C and subsequently stored at 110 °C before use. The mixtures were homogenized in an agate mortar under acetone for 45 min, and trace elements were added to the oxide mixture as ICP-MS standard solutions. Cr was also added from a standard solution. The trace element-bearing mixture was dried in a 110 °C furnace and then fired in a platinum crucible at 800 °C overnight for decarbonation. Subsequently, the mixture was vitrified at 1600 °C for 1 h. The resulting glass was crushed and homogenized again for 45 min in an agate mortar. The melting procedure was repeated to ensure homogeneous distribution of trace elements in the starting material glasses. To minimize iron loss to the crucible during the glass preparation, iron was added as Fe_2O_3 after the second melting step, after which the mixes were homogenized once again.

Table 1 Major element compositions of starting materials

Sample	sp2	sp4	sp5	sp6
n	9	13	20	21
MgO	13.9 ± 0.2	13.7 ± 0.1	10.2 ± 0.2	6.8 ± 0.1
SiO_2	42.6 ± 0.4	42.0 ± 0.3	40.4 ± 0.4	38.2 ± 0.3
CaO	22.7 ± 0.3	21.8 ± 0.3	20.6 ± 0.3	19.5 ± 0.3
Al_2O_3	18.9 ± 0.2	18.6 ± 0.2	17.8 ± 0.3	16.9 ± 0.2
TiO_2		2.0 ± 0.1	1.9 ± 0.1	1.8 ± 0.1
FeO*			7.5 ± 0.3	15.0 ± 0.2
Total	98.1 ± 0.7	98.1 ± 0.5	98.5 ± 0.7	98.3 ± 0.6

n number of measurements

* FeO total

Starting compositions sp10, sp12, sp14 and sp15 are the same as sp2, sp4, sp5 and sp6, respectively, with 500 (sp12) or 2000 ppm (sp10, sp14, sp15) Cr added from a standard solution. Starting composition prg has the same composition as sp4, but with no trace elements added. This starting mixture was not made into a glass but left as an oxide mixture. Uncertainties are given as 1σ standard deviation

Experimental techniques

Experiments were conducted in a vertical tube furnaces (GERO, Germany) equipped for gas mixing, using Tylan mass flow controllers. The oxygen fugacity was buffered using mixtures of CO and CO_2 gas (Deines et al. 1976). Small amounts of starting powder were mixed with an organic glue and suspended on a thin platinum wire loop of either Pt_{100} (0.05 mm diameter) or $Pt_{94}Rh_6$ composition (0.1 mm diameter). The loops are about 3 mm in diameter, and several samples could be suspended from a self-made platinum wire sample holder to run multiple samples

Table 2 Experimental conditions and run products

Run nr.	Start mat.	Sample	T (°C)	Log fO_2	ΔQFM	Phases present
1	sp2	sp2_05	1300	−0.7	6.5	gl, sp
2	sp4	sp4_01	1310	−0.7	6.4	gl, sp
3	sp4	sp4_02	1300	−8	−0.8	gl, sp
4	sp4	sp4_03	1250	−8	−0.3	gl, sp, ol
	sp5	sp5_02	1250	−8	−0.3	gl, sp
5	sp5	sp5_03	1220	−8	0.1	gl, sp
	sp6	sp6_03	1220	−8	0.1	gl, sp, pl
6	sp6	sp6_04	1220	−10	−1.9	gl, sp
7	sp5	sp5_05	1250	−10	−2.3	gl, sp
8	sp6	sp6_06	1200	−10	−1.7	gl, sp
9	sp5	sp5_07	1220	−12	−3.9	gl, sp, ol, pl, minor cpx
	sp6	sp6_07	1220	−12	−3.9	gl, sp, pl
10	sp5	sp5_08	1250	−12	−4.3	gl, sp, pl
11	sp2	sp2_10	1320	−0.7	6.3	gl, sp
	sp4	sp4_10	1320	−0.7	6.3	gl, sp
12	sp6	sp6_08	1220	−6	2.1	gl, sp, pl
13	sp5	sp5_10	1220	−10	−1.9	gl, sp, ol, pl
	sp6	sp6_09	1220	−10	−1.9	gl, sp, pl
14	sp4	sp4_13	1320	−4	3.0	gl, sp
15	sp10	sp10_02	1430	−4	2.0	gl, sp
16	sp12	sp12_01	1350	−8	1.3	gl, sp
	sp14	sp14_01	1350	−8	1.3	gl, sp
	sp15	sp15_01	1350	−8	1.3	gl, sp
17	sp12	sp12_02a	1320	−4	3.0	gl, sp
	sp12	sp12_02b	1320	−4	3.0	gl, sp
18	prg	prg11	1300	−0.7	6.5	gl, sp
	prg	prg12	1300	−0.7	6.5	gl, sp
	sp4	sp4_18	1300	−0.7	6.5	gl, sp
19	prg	prg13	1300	−10	−2.8	gl, sp
	prg	prg14	1300	−10	−2.8	gl, sp
	sp4	sp4_19	1300	−10	−2.8	gl, sp

Phases present: *gl* glass, *sp* spinel, *ol* olivine, *pl* plagioclase, *cpx* clinopyroxene. Run duration was typically 48 h for each experiment, except run nr1 (20 h) nr2 (72 h) nr3 (20 h), and run 18 and 19 (24 h)

simultaneously. The samples were lowered in the hot zone of the furnace at 800 °C, then heated up to at least 50 °C above the liquidus temperature. The samples were kept at this temperature for 30 min to ensure that they were completely molten. After this, the samples were cooled relatively fast (2.5 °C/min) to temperatures around or slightly below the liquidus temperature, and further cooled (more slowly, with 1 °C/h) to the final run temperature. To facilitate spinel growth, the temperature was repeatedly increased and slowly cooled over a small temperature interval, and after this kept at the final temperature for at least 12 h. The total run time was typically around 48 h. The samples were quenched rapidly by dropping them into water. Details of all experimental runs are given in Table 2. The samples were mounted in epoxy resin, polished and examined using optical microscopy and a JEOL 6610LV scanning electron microscope equipped with an EDX system. Samples that contained spinels large enough for chemical characterization were subsequently analyzed for major and trace elements using electron microprobe and laser ablation ICP-MS.

Analytical procedures

Major element analysis

Major element analyses on the glasses and all crystal phases were performed with a JEOL JXA-8900 M electron microprobe, using an acceleration voltage of 15 kV. Natural and synthetic standard reference materials that were used are Cr_2O_3 (Cr), rutile (Ti), hypersthene (Si), kyanite (Al), diopside (Ca), olivine (Mg) and fayalite (Fe). A number of

secondary reference materials (chromite, olivine, Cr-diopside) were measured as unknowns to monitor external precision and accuracy. Mineral phases were analyzed with a focused beam and a beam current of 15 nA, and counting times were 20 s on the peak and 10 s on the background. The glasses were analyzed with a 10 μm defocused spot, a beam current of 5 nA, and counting times of 10 s on the peak and 5 s on the backgrounds. The spinel and glass major element data are presented in Table 3.

Trace element analysis

Trace elements were measured by a Thermo Scientific Element 2 sector field ICP-MS coupled to a New Wave UP193HE ArF Excimer laser, operating with a ca. 5 J/cm^2 beam intensity and a repetition rate of 10 Hz. A large volume ablation cell with fast signal response and short wash out times (<1 s) was used. The cell holds up to ten 1-inch-diameter mounts, six thin sections and additional reference materials. Prior to sample analysis, the system was tuned with the NIST SRM 612 reference glass standard for high sensitivity, stability and low oxide rates (^{232}Th^{16}O/^{232}Th < 0.2 %). Spot sizes for the spinel analyses were between 12 and 60 μm in diameter, but in most cases 35 μm, as this proved to be the best compromise between a sufficient diameter for a good mass spectrometer signal, and a small enough diameter to avoid melt inclusions that were sometimes present in the spinel. Glasses were measured with a spot size of 35 or 60 μm. The signal ablation time was 40 s for the peak and 20 s for the background. Wash out time between individual spots was 10 s.

The NIST SRM 612 glass (Jochum et al. 2011) was used as an external standard and the BIR-1G glass (Jochum et al. 2005) as an unknown to monitor precision and accuracy. Five to ten sample measurements were always bracketed by three measurements of the NIST 612 glass and two measurements of the BIR-1G glass. ^{43}Ca was used as an internal standard calibration for the glass and the plagioclase measurements, and ^{29}Si was used for olivine. Spinel does not contain large amounts of Ca or Si, elements which are commonly employed as internal standards during LA-ICP-MS analysis. After some experimentation, ^{47}Ti proved to be the most suitable isotope to use as an internal standard for spinel measurements (see also Page and Barnes (2009) who came to the same conclusion). Therefore, TiO_2 was added to most of starting compositions for use as an internal standard for spinel measurements. In a few samples with low titanium (composition Sp2 and Sp10), ^{26}Mg was used as an internal standard instead. Trace element concentrations were calculated using the Glitter software (Jackson 2001). To avoid melt contamination during the measurements of the spinel crystals, we took special care to avoid U and Th spikes in the LA-ICP-MS signal during spinel measurements, since U and Th are very incompatible in spinel and can be used to monitor possible cross-contamination of spinel analyses. The raw trace element data for all measurements are shown in the electronic supplement.

The analyses of Sc, Co, V, Cr, Mn, Ga, Lu and the HFSEs gave very reliable and consistent results. The analyses of some of the other elements show somewhat larger uncertainties (see Table 4), because of high background counts (Cr, Ni) or low concentrations in the spinel (Y, W, U, Th).

The measurements of Pt and Rh are complicated due to the fact that platinum group elements have the tendency to form the so-called (nano-)nuggets, which are small, often nanoscale phases of either PGE-bearing minerals or alloys (Brenan et al. 2012; Ertel et al. 1999; Fortenfant et al. 2003). If these nuggets are large enough, they show up during the laser ablation measurements as high Pt and Rh peaks. In principle, the laser ablation technique is a well-suited method to filter out these peaks. However, in some cases, the nuggets may be too small or too numerous to be detected as isolated spikes during the time resolved analysis, in which case the PGE concentrations may be overestimated. The issue this poses for the determination of partition coefficients is discussed in the PGE section in this paper.

TEM analysis

We prepared an electron transparent lamella mount from one sample for further investigations by transmission electron microscopy (TEM) to locate possible nano-nuggets in the spinel. The sample was initially thinned by conventional Ar ion milling using a Gatan DuoMill 600 at 5 kV and 17° incidence angle. Further thinning to final electron transparency (~150 nm) was performed on a focused ion beam–scanning electron microscope (FIB-SEM) using a Zeiss CrossBeam™ 1540 EsB with 30 kV Ga^+ ions and 50 pA beam current until final electron transparency was obtained. TEM investigations were performed on a Zeiss Libra 200FE operated with a Schottky field emission electron source at 200 kV acceleration voltage, a Köhler illumination system, and an in-column Omega energy filter applying standard imaging techniques (brightfield imaging, high-resolution TEM) and analytical X-ray spectrometry (Noran Si(Li) EDX detector). The lamella was also analyzed in scanning TEM mode using a high angle annular darkfield (HAADF) detector to discriminate possible high-Z nuggets at high spatial resolution (a few nm) from the surrounding low-Z spinel (Z: atomic number).

Table 3 Spinel and glass major element compositions of all experiments

Sample	sp4_01		sp4_10		Sp4_13		sp4_02		sp4_03	
T (°C)	1300		1320		1320		1300		1250	
Log fO_2	−0.7		−0.7		−4		−8		−8	
ΔQFM	6.4		6.3		3.0		−0.8		−0.3	
Phase	Spinel	Glass	Spinel	Glass	Spinel	Glass	Spinel	Glass	Spinel	Glass
n	4	15	6	10	5	7	21	12	4	12
MgO	27.5 ± 0.2	13.5 ± 0.1	27.1 ± 0.3	13.5 ± 0.1	26.7 ± 0.2	13.8 ± 0.2	27.3 ± 0.2	13.5 ± 0.2	27.3 ± 0.2	11.7 ± 0.2
SiO_2	0.1 ± 0.01	42.4 ± 0.4	0.09 ± 0.01	42.3 ± 0.1	0.09 ± 0.02	42.4 ± 0.3	0.10 ± 0.01	42.8 ± 0.2	0.1 ± 0.02	42.7 ± 0.3
CaO	≤0.01	21.9 ± 0.3	≤0.01	21.7 ± 0.2	≤0.02	21.6 ± 0.3	≤0.05	22.0 ± 0.4	≤0.03	23.0 ± 0.4
Cr_2O_3	0.12 ± 0.02	≤0.01	≤0.03	≤0.01	3.1 ± 0.1	≤0.02	0.8 ± 0.2	≤0.01	0.6 ± 0.3	≤0.02
Al_2O_3	70.9 ± 0.2	18.4 ± 0.2	70.1 ± 0.3	18.2 ± 0.2	67.9 ± 0.7	18.6 ± 0.2	70.0 ± 0.4	18.1 ± 0.1	69.9 ± 1.0	18.3 ± 0.2
TiO_2	0.16 ± 0.02	2.00 ± 0.07	0.14 ± 0.02	2.00 ± 0.03	0.15 ± 0.03	2.00 ± 0.15	0.17 ± 0.02	2.0 ± 0.1	0.15 ± 0.03	2.07 ± 0.06
FeO*	≤0.04	≤0.05	≤0.04	≤0.02	≤0.03	≤0.01	≤0.01	≤0.02	≤0.03	≤0.02
Total	98.8 ± 0.1	98.2 ± 0.5	97.47 ± 0.4	97.7 ± 0.4	98.0 ± 0.6	98.5 ± 0.6	98.4 ± 0.3	98.4 ± 0.4	98.1 ± 0.9	97.9 ± 0.6
Mg	0.98		0.98		0.97		0.98		0.98	
Si	0.00		0.00		0.00		0.00		0.00	
Ca	0.00		0.00		0.00		0.00		0.00	
Cr	0.00		0.00		0.06		0.02		0.01	
Al	2.00		2.01		1.95		1.99		1.99	
Ti	0.00		0.00		0.00		0.00		0.00	
Fe*	0.00		0.00		0.00		0.00		0.00	
Total	2.99		2.99		2.99		2.99		2.99	
Fe^{2+} [a]	0.00		0.00		0.00		0.00		0.00	
Fe^{3+} [b]	0.00		0.00		0.00		0.00		0.00	
Mg# [c]	1.00		1.00		1.00		1.00		1.00	
Cr# [d]	0.00		0.00		0.03		0.01		0.01	

Table 3 continued

Sample	sp4_18		sp4_19		sp5_02		sp5_03		sp5_05	
T (°C)	1300		1300		1250		1220		1250	
Log fO_2	−0.7		−10		−8		−8		−8	
ΔQFM	6.5		−2.8		−0.3		0.1		−2.3	
Phase	Spinel	Glass	Spinel	Glass	Spinel	Glass	Spinel	Glass	Spinel	Glass
n	8	14	9	10	10	9	19	12	17	10
MgO	28 ± 0.2	13.4 ± 0.1	28.2 ± 0.4	13.9 ± 0.1	23.3 ± 0.3	10 ± 0.1	22.9 ± 0.3	9.5 ± 0.2	23.7 ± 0.2	10 ± 0.1
SiO_2	0.09 ± 0.01	42.4 ± 0.2	0.09 ± 0.01	42.1 ± 0.1	0.08 ± 0.01	40.6 ± 0.3	0.09 ± 0.02	40.8 ± 0.4	0.08 ± 0.01	40.7 ± 0.2
CaO	≤0.02	21.9 ± 0.2	≤0.03	21.8 ± 0.2	≤0.03	20.8 ± 0.2	≤0.02	21.0 ± 0.3	≤0.02	20.8 ± 0.1
Cr_2O_3	≤0.01	≤0.01	0.6 ± 0.1	≤0.02	1.1 ± 0.5	≤0.03	≤0.49	≤0.02	1.2 ± 0.5	≤0.01
Al_2O_3	71.1 ± 0.4	18.5 ± 0.2	70.5 ± 0.9	18.6 ± 0.1	66.1 ± 0.8	17.2 ± 0.1	65.5 ± 0.6	15.9 ± 0.3	66.8 ± 0.5	17.2 ± 0.1
TiO_2	0.16 ± 0.01	2.03 ± 0.06	0.17 ± 0.03	1.97 ± 0.06	0.19 ± 0.01	1.85 ± 0.09	0.20 ± 0.03	1.92 ± 0.12	0.18 ± 0.02	1.95 ± 0.05
FeO*	0.05 ± 0.02	≤0.02	≤0.01	≤0.02	8.4 ± 0.1	7.7 ± 0.1	10.0 ± 0.3	8.7 ± 0.1	7.1 ± 0.1	7.3 ± 0.1
Total	99.5 ± 0.3	98 ± 0.3	99.7 ± 0.6	98.3 ± 0.4	99.2 ± 0.3	98.1 ± 0.4	99.2 ± 0.4	97.8 ± 0.6	99.0 ± 0.3	98 ± 0.4
Mg	0.99		1.00		0.87		0.86		0.88	
Si	0.00		0.00		0.00		0.00		0.00	
Ca	0.00		0.00		0.00		0.00		0.00	
Cr	0.00		0.01		0.02		0.01		0.02	
Al	2.00		1.98		1.94		1.94		1.95	
Ti	0.00		0.00		0.00		0.00		0.00	
Fe*	0.00		0.00		0.18		0.21		0.15	
Total	3.00		3.00		3.01		3.02		3.01	
Fe^{2+} [a]	0.00		0.00		0.15		0.17		0.13	
Fe^{3+} [b]	0.00		0.00		0.03		0.04		0.02	
Mg# [c]	1.00		1.00		0.85		0.84		0.87	
Cr# [d]	0.00		0.01		0.01		0.01		0.01	

Table 3 continued

Sample	sp5_10		sp5_08		sp5_07		sp6_08		sp6_03	
T (°C)	1220		1250		1220		1220		1220	
Log fO_2	−10		−12		−12		−6		−8	
ΔQFM	−1.9		−4.3		−3.9		2.1		0.1	
Phase	Spinel	Glass	Spinel	Glass	Spinel	Glass	Spinel	Glass	Spinel	Glass
n	12	10	8	9	5	10	10	15	14	
MgO	23.7 ± 0.2	9.9 ± 0.3	24.3 ± 0.3	11.2 ± 0.1	23.6 ± 0.2	9.7 ± 0.2	10.9 ± 0.7	7.4 ± 0.1	17.5 ± 0.2	6.8 ± 0.1
SiO_2	0.11 ± 0.01	40.6 ± 0.3	0.08 ± 0.01	41.0 ± 0.3	0.10 ± 0.01	40.7 ± 0.4	0.11 ± 0.0	39 ± 0.3	0.08 ± 0.0	38.6 ± 0.3
CaO	≤0.02	22.8 ± 0.3	≤0.02	21.3 ± 0.1	≤0.04	23.3 ± 0.1	≤0.09	19.9 ± 0.2	≤0.03	19.8 ± 0.2
Cr_2O_3	1.4 ± 0.4	≤0.01	1.14	0.09	0.02	1.2 ± 0.2	≤0.02	0.07 ± 0.03	≤0.01	1.01 ± 0.5
Al_2O_3	66.3 ± 0.5	14.3 ± 0.2	67.8 ± 0.3	16.1 ± 0.1	66.8 ± 0.2	14.2 ± 0.2	22.5 ± 3.1	12.9 ± 0.1	59.8 ± 0.6	14.9 ± 0.1
TiO_2	0.27 ± 0.03	2.6 ± 0.1	0.23 ± 0.03	2.15 ± 0.1	0.19 ± 0.03	2.81 ± 0.1	1.97 ± 0.2	2.05 ± 0.04	0.27 ± 0.03	1.92 ± 0.07
FeO*	6.9 ± 0.1	7.9 ± 0.1	5.6 ± 0.3	6.19 ± 0.03	6.5 ± 0.1	7.6 ± 0.4	62.4 ± 3.1	16.5 ± 0.2	21.2 ± 0.3	15.9 ± 0.3
Total	98.6 ± 0.6	98.1 ± 0.6	99.1 ± 0.3	98.0 ± 0.2	98.5 ± 0.2	98.3 ± 0.5	98.0 ± 0.6	97.7 ± 0.7	99.9 ± 0.5	97.9 ± 0.4
Mg	0.88		0.89		0.88		0.50		0.69	
Si	0.00		0.00		0.00		0.00		0.00	
Ca	0.00		0.00		0.00		0.00		0.00	
Cr	0.03		0.02		0.02		0.00		0.02	
Al	1.95		1.97		1.96		0.82		1.86	
Ti	0.01		0.00		0.00		0.05		0.01	
Fe*	0.14		0.12		0.14		1.62		0.47	
Total	3.01		3.00		3.00		3.00		3.05	
Fe^{2+} [a]	0.13		0.11		0.13		0.54		0.36	
Fe^{3+} [b]	0.02		0.00		0.01		1.08		0.11	
Mg# [c]	0.87		0.89		0.87		0.48		0.66	
Cr# [d]	0.01		0.01		0.01		0.00		0.01	

Table 3 continued

Sample	sp6_04		sp6_09		sp6_06		sp6_07		sp12_01	
T (°C)	1220		1220		1200		1220		1350	
Log fO_2	−10		−10		−10		−12		−8	
ΔQFM	−1.9		−1.9		−1.7		−3.9		1.3	
Phase	Spinel	Glass	Spinel	Glass	Spinel	Glass	Spinel	Glass	Spinel	Glass
n	7	10	7	10	9	10	5	10	6	7
MgO	17.7 ± 0.1	6.6 ± 0.2	18.3 ± 0.1	7.7 ± 0.1	18.2 ± 0.2	7.3 ± 0.1	18.5 ± 0.2	8 ± 0.1	26.3 ± 0.2	13.8 ± 0.2
SiO_2	0.05 ± 0.02	38.6 ± 0.2	0.07 ± 0.01	38.6 ± 0.2	0.06 ± 0.01	38.3 ± 0.3	0.07 ± 0.01	38.9 ± 0.3	0.08 ± 0.02	42.1 ± 0.3
CaO	≤0.02	19.5 ± 0.1	≤0.05	19.6 ± 0.2	≤0.06	19.6 ± 0.2	0.06 ± 0.04	19.8 ± 0.2	0.06 ± 0.1	21.5 ± 0.1
Cr_2O_3	1.26 ± 0.6	≤0.01	1.39 ± 0.36	≤0.02	≤0.7	≤0.02	1.74 ± 0.07	≤0.03	8.4 ± 0.5	0.06 ± 0.01
Al_2O_3	63.2 ± 0.6	15.9 ± 0.1	63.5 ± 0.4	14.5 ± 0.1	63.1 ± 0.6	14.0 ± 0.2	64.1 ± 0.2	14.7 ± 0.1	63.6 ± 0.5	18.8 ± 0.1
TiO_2	0.23 ± 0.03	1.83 ± 0.05	0.28 ± 0.04	2.07 ± 0.02	0.23 ± 0.02	2.02 ± 0.1	0.30 ± 0.02	2.10 ± 0.05	0.20 ± 0.02	2.0 ± 0.1
FeO*	17.2 ± 0.2	15.5 ± 0.2	16.7 ± 0.1	15.8 ± 0.1	16.9 ± 0.4	15.9 ± 0.2	14.3 ± 0.1	15.1 ± 0.1	≤0.01	≤0.01
Total	99.7 ± 0.4	97.9 ± 0.3	100.2 ± 0.3	98.3 ± 0.4	99.3 ± 0.7	97.2 ± 0.3	99.1 ± 0.4	98.6 ± 0.5	98.6 ± 0.3	98.3 ± 0.6
Mg	0.68		0.70		0.70		0.71		0.97	
Si	0.00		0.00		0.00		0.00		0.00	
Ca	0.00		0.00		0.00		0.00		0.00	
Cr	0.03		0.03		0.01		0.04		0.16	
Al	1.93		1.92		1.93		1.94		1.85	
Ti	0.01		0.01		0.01		0.01		0.00	
Fe*	0.37		0.36		0.37		0.31		0.00	
Total	3.02		3.02		3.02		3.00		2.99	
Fe^{2+} [a]	0.34		0.32		0.32		0.30		0.00	
Fe^{3+} [b]	0.04		0.04		0.05		0.01		0.00	
Mg# [c]	0.67		0.69		0.69		0.71		1.00	
Cr# [d]	0.01		0.01		0.01		0.02		0.08	

Table 3 continued

Sample	sp12_02a		sp12_02b		sp10_02		sp14_01		sp15_01	
T (°C)	1320		1320		1430		1350		1350	
Log fO_2	−4		−4		−4		−8		−8	
ΔQFM	3.0		3.0		2.0		1.3		1.3	
Phase	Spinel	Glass	Spinel	Glass	Spinel	Glass	Spinel	Glass	Spinel	Glass
n	6	7	10	6	6	6	26	6	10	7
MgO	26.8 ± 0.4	13.3 ± 0.3	26.6 ± 0.3	13.5 ± 0.2	24.6 ± 0.2	13.4 ± 0.2	20.3 ± 0.6	9.9 ± 0.1	14.2 ± 0.5	6.8 ± 0.1
SiO_2	0.09 ± 0.01	42.6 ± 0.3	0.09 ± 0.02	42.9 ± 0.4	0.08 ± 0.01	43.3 ± 0.2	0.07 ± 0.02	40.8 ± 0.2	0.07 ± 0.03	39.0 ± 0.4
CaO	0.07 ± 0.03	21.9 ± 0.2	≤0.05	21.8 ± 0.3	0.21 ± 0.08	22.1 ± 0.1	0.07 ± 0.03	20.1 ± 0.1	0.11 ± 0.04	19.3 ± 0.4
Cr_2O_3	5.95 ± 0.5	≤0.03	6.38 ± 0.75	0.05 ± 0.03	30.2 ± 1.1	0.17 ± 0.06	21.0 ± 3.6	0.06 ± 0.04	26.0 ± 3.7	0.10 ± 0.06
Al_2O_3	65.5 ± 0.8	18.1 ± 0.2	65.9 ± 0.8	18.3 ± 0.3	43.9 ± 1.3	19.2 ± 0.2	48.2 ± 3.2	17.7 ± 0.2	39.4 ± 3.7	17.2 ± 0.2
TiO_2	0.18 ± 0.02	2.1 ± 0.1	0.17 ± 0.02	2.0 ± 0.1	≤0.01	0.09 ± 0.02	0.31 ± 0.03	2.0 ± 0.1	0.41 ± 0.02	1.83 ± 0.08
FeO*	0.04 ± 0.01	≤0.03	0.03 ± 0.01	≤0.05	≤0.01	≤0.02	9.5 ± 0.3	7.6 ± 0.1	20.2 ± 0.3	14.0 ± 0.2
Total	98.7 ± 0.5	98.2 ± 0.6	99.2 ± 0.3	98.8 ± 0.7	98.9 ± 0.3	98.4 ± 0.3	99.5 ± 0.4	98.3 ± 0.5	100.3 ± 0.5	98.3 ± 0.7
Mg	0.98		0.97		0.97		0.81		0.61	
Si	0.00		0.00		0.00		0.00		0.00	
Ca	0.00		0.00		0.01		0.00		0.00	
Cr	0.12		0.12		0.63		0.45		0.59	
Al	1.89		1.89		1.38		1.52		1.33	
Ti	0.00		0.00		0.00		0.01		0.01	
Fe*	0.00		0.00		0.00		0.21		0.48	
Total	2.99		2.99		2.99		3.01		3.03	
Fe^{2+} [a]	0.00		0.00		0.00		0.20		0.43	
Fe^{3+} [b]	0.00		0.00		0.00		0.02		0.06	
Mg# [c]	1.00		1.00		1.00		0.81		0.59	
Cr# [d]	0.06		0.06		0.32		0.23		0.31	

Table 3 continued

Sample	sp2_05		prg11		prg12		prg13		prg14	
T (°C)	1300		1300		1300		1300		1300	
Log fO_2	–0.7		–0.7		–0.7		–10		–10	
ΔQFM	6.5		6.5		6.5		–2.8		–2.8	
Phase	Spinel	Glass	Spinel	Glass	Spinel	Glass	Spinel	Glass	Spinel	Glass
n	9	14	10	14	7	10	11	10		
MgO	28 ± 0.2	12.7 ± 0.1	27.9 ± 0.4	13.4 ± 0.1	27.9 ± 0.3	13.5 ± 0.1	27.9 ± 0.5	13.7 ± 0.1	28.1 ± 0.1	13.5 ± 0.1
SiO_2	0.08 ± 0.01	44.3 ± 0.1	0.10 ± 0.02	41.6 ± 0.2	0.09 ± 0.01	41.8 ± 0.2	0.09 ± 0.01	41.9 ± 0.2	0.09 ± 0.01	42.0 ± 0.2
CaO	≤0.05	23.4 ± 0.1	≤0.03	22.6 ± 0.2	≤0.02	22.6 ± 0.2	≤0.02	22.5 ± 0.2	≤0.02	22.7 ± 0.1
Cr_2O_3	≤0.2	≤0.02	≤0.01	≤0.01	≤0.02	≤0.01	≤0.02	≤0.01	≤0.02	≤0.01
Al_2O_3	71.6 ± 0.7	18.9 ± 0.2	70.4 ± 0.9	18.0 ± 0.2	70.3 ± 0.7	17.8 ± 0.2	70.9 ± 1.3	18.3 ± 0.1	71.1 ± 0.3	18.0 ± 0.1
TiO_2	0.17 ± 0.04	2.07 ± 0.05	0.16 ± 0.03	2.1 ± 0.1	0.17 ± 0.03	2.07 ± 0.05	0.18 ± 0.03	2.1 ± 0.1		
FeO*	0.06 ± 0.02	≤0.03	0.06 ± 0.02	≤0.03	≤0.01	≤0.01	≤0.01	≤0.02		
Total	100.0 ± 0.7	99.3 ± 0.3	98.8 ± 0.6	97.7 ± 0.4	99.2 ± 0.4	97.8 ± 0.5	99.2 ± 1.0	98.5 ± 0.4	99.5 ± 0.4	98.3 ± 0.4
Mg	0.99		1.00		1.00		0.99		1.00	
Si	0.00		0.00		0.00		0.00		0.00	
Ca	0.00		0.00		0.00		0.00		0.00	
Cr	0.00		0.00		0.00		0.00		0.00	
Al	2.00		1.99		1.99		2.00		2.00	
Ti	0.00		0.00		0.00		0.00			
Fe*	0.00		0.00		0.00		0.00			
Total	3.00		3.00		3.00		3.00		3.00	
Fe^{2+} [a]	0.00		0.00		0.00		0.00		0.00	
Fe^{3+} [b]	0.00		0.00		0.00		0.00		0.00	
Mg# [c]	1.00		1.00		1.00		1.00		1.00	
Cr# [d]	0.00		0.00		0.00		0.00		0.00	

Uncertainties are given as 1σ standard deviation

* FeO or Fe total

[a, b] Fe^{2+} and Fe^{3+} are calculated from spinel stoichiometry, [c] Mg# is $Mg/(Mg + Fe^{2+})$, [d] Cr# is $Cr/(Cr + Al)$

Results

Experimental results

All experimental run products contain glass and spinels, some runs contain additional phases such as olivine, plagioclase or clinopyroxene (cpx). Two SEM backscatter images of typical run products are shown in Fig. 1a, b. Table 2 lists all phases present in the experimental run products. The spinels are typically idiomorphic, ca. 50 µm across, but their sizes range from 20 to 300 µm. Interestingly, the spinels appear to nucleate preferably either close to or in contact with the platinum wire. The spinels of nearly pure $MgAl_2O_4$ composition are transparent and colorless, while the spinels containing iron are dark purple or dark brown, and spinels with chromium are purple in color.

Spinel is the liquidus phase in all bulk compositions and for every fO_2. The liquidus temperatures of the different starting materials vary and are critically dependent on composition; it is around 1300 °C in the Fe- and Cr-free composition, and in the Fe-rich experiments it is lower (around 1250 °C), and it strongly increases when Cr is present. In high-Cr compositions (2 wt% Cr_2O_3), the liquidus temperature is very high (probably >1600 °C). In these cases, we could not prepare completely homogenous glasses from our starting material mixtures; these glasses always contain small crystals of spinel or eskolaite. This poses a problem for growing large (>20 µm) crystals; if any crystalline nuclei are left in the starting mix, new spinel crystals nucleate rapidly, but the growth rates are small. Therefore, only the starting compositions with lower Cr concentration yielded sufficiently large spinels.

When present, plagioclase appears idiomorphic, often platy and typically several hundred µm across. Olivines are either idiomorphic or show skeleton textures, and are sometimes intergrown with plagioclase. Cpx is idiomorphic. The presence of mineral phases in addition to spinel depends on the composition of the starting material. The Fe-free and low-Fe (sp4 and sp5) starting materials crystallized olivine as the second phase to appear after spinel, and at lower temperatures, plagioclase and cpx are present in these runs. Composition sp6 (with 10 wt% FeO) contains only plagioclase as an additional mineral phase, and no olivine is present. In the Cr-bearing experiments, spinel was the only mineral phase present.

Melts in all runs were quenched into a homogeneous glass without any detectable quench crystals. In two of the iron-bearing experiments, a minute amount of a second, immiscible silicate liquid was present. Due to the small size of the immiscible droplets (<1 µm), quantitative analysis of the second liquid was not possible.

Analytical results

Major elements

Detailed spinel and glass compositions are given in Table 3. The range of spinel compositions is shown in Fig. 2a, b. The compositions of the other minerals are shown in table 6 of the electronic supplements. Spinel compositions range from nearly pure $MgAl_2O_4$ spinel to spinel solid solutions with a significant hercynite ($FeAl_2O_4$) component (11–57 %) or Mg-chromite ($MgCr_2O_4$) component (6–32 %). One sample (sp6_08) has a magnetite (Fe_3O_4) component of 54 %. The spinels are usually homogenous in terms of major elements except the spinels in run sp6_08 which are rich in Fe^{3+} (Table 3). This experiment was performed under a relatively high oxygen fugacity (log $fO_2 = -6$). The spinels in Sp6_08 are strongly zoned in Fe and Al, most consisting of an Al-rich core with a wide rim of iron-rich spinel. The Al-rich cores were most likely formed early in the experimental run, during the fast cooling segment, during which the oxygen fugacity was not as well controlled. The Fe-rich rims are most probably formed during the final run conditions; hence, we assume that the rims are equilibrated with the melt. These rims were large enough to measure with LA-ICP-MS. Some of the Cr-rich spinels show a slight zonation in Cr–Al. This, however, does not affect the other major element or the trace elements composition, both of which were homogenously distributed.

The olivine compositions are pure forsterite in all Fe-free compositions. Olivines in the Fe-bearing experiments contain a fayalite component of around 10 % (see table 6 electronic supplements). Plagioclase in all runs is nearly pure anorthite. Cpx has a high augite content with very high Al_2O_3 and TiO_2 concentrations, and is often not well equilibrated, which is evident from patchy zoning in Al and Ti. As cpx takes up a large proportion of most trace elements, these experiments are probably compromised; therefore, the cpx-bearing experiments are not used to calculate partition coefficients. Similarly, the experiments with low glass content (less than ~50 %) were discarded because of the possibility of melt pockets in these experiments which might not be in equilibrium with the entire sample. When excluding the runs with low glass content, glasses are always homogenous in major element composition, regardless of bulk compositions or temperature.

Trace elements

Trace element concentrations for spinel and glass, as well as the spinel partition coefficients are shown in Table 4. For each sample, we analyzed five spots in the melt, and

Table 4 Analytical results of the trace element analyses of glasses and spinel, and spinel partition coefficients

Composition	sp4			sp4			sp4		
Sample	sp4_01			sp4_10			Sp4_13		
T (°C)	1310			1320			1320		
Log fO_2	−0.7			−0.7			−4		
ΔQFM	6.4			6.3			3.0		
	Spinel	Glass	D_{sp}	Spinel	Glass	D_{sp}	Spinel	Glass	D_{sp}
n	3	3	3	2	5	2	2	5	2
Si	532 ± 57	220945 ± 4677	0.0024 ± 0.0006	532 ± 52	213098 ± 3597	0.0025 ± 0.0002	754	196259 ± 3263	0.00384
Ca	998 ± 207	164481	0.006	792 ± 191	156963	0.005 ± 0.001	b.d.l	154283	
Sc	1.0 ± 0.2	26.5 ± 0.3	0.038 ± 0.001	0.9 ± 0.2	24.7 ± 0.3	0.036 ± 0.007	0.94 ± 0.35	23.7 ± 0.3	0.039 ± 0.015
Ti	925 ± 24	14654 ± 117	0.063 ± 0.001	851 ± 31	13570 ± 159	0.063 ± 0.002	888 ± 23	12824 ± 293	0.069 ± 0.002
V	b.d.l	27.2 ± 1.4		b.d.l	27.2 ± 0.6		0.8 ± 0.2	23 ± 0.8	0.033 ± 0.007
Cr	764 ± 114	b.d.l		181 ± 9	b.d.l		21197 ± 1549	107 ± 3.9	198 ± 16
Mn	29.0 ± 1.3	49.6 ± 0.6	0.58 ± 0.02	26.8 ± 2.2	46.6 ± 0.7	0.57 ± 0.05	22.1 ± 1.7	43.6 ± 0.4	0.51 ± 0.04
Co	65.6 ± 0.5	25.4 ± 0.7	2.6 ± 0.1	60.8 ± 5.9	23.7 ± 0.4	2.6 ± 0.3	66.9 ± 0.4	22.2 ± 0.6	3.01 ± 0.09
Ni	331 ± 17	57.7 ± 2.4	5.7 ± 0.3	259 ± 31	39.6 ± 3.0	6.5 ± 0.9	192 ± 10	22.6 ± 3.9	8.49996 ± 1.5
Cu	244 ± 24	760.8 ± 0.1	0.32	115 ± 11	481.2 ± 7.9	0.24 ± 0.02	7.8 ± 0.3	71.7 ± 1.8	0.109 ± 0.005
Zn	122.5 ± 4.5	24.0 ± 0.4	5.1	145 ± 12	27 ± 0.9	5.4 ± 0.5	nd	nd	nd
Ga	116.4 ± 4.2	25.8 ± 0.5	4.5 ± 0.1	110.5 ± 9.4	26.7 ± 0.9	4.1 ± 0.4	116.1 ± 0.8	22.2 ± 0.4	5.2 ± 0.1
Y	b.d.l	107.5 ± 2.1		b.d.l	103.4 ± 1.4		b.d.l	97 ± 0.5	b.d.l
Zr	0.05 ± 0.01	126.8 ± 4.9	0.0004 ± 0.00007	0.06	120.4 ± 1.3	0.0005	0.11	114.4 ± 2.9	0.00098
Nb	0.06	114.8 ± 2.0	0.0006	0.03 ± 0.01	107.4 ± 1.4	0.0003 ± 0.0001	0.04	103.1 ± 2.4	0.00039
Mo	0.05 ± 0.02	14.9 ± 0.8	0.003 ± 0.002	b.d.l	15.2 ± 0.4		b.d.l	162.6 ± 3.9	
Rh	17.4 ± 1.0	0.77 ± 0.25	22.5 ± 7.5	1099 ± 298	2.6 ± 0.2	431 ± 122	34.6 ± 4.2	0.36 ± 0.16	97 ± 46
Lu	0.028 ± 0.009	95.1 ± 1.7	0.0003 ± 0.00005	0.029 ± 0.006	92.8 ± 0.9	0.0003 ± 0.00006	0.044	83.9 ± 2	0.00052
Hf	0.08 ± 0.03	92.1 ± 0.5	0.0009 ± 0.0001	0.07 ± 0.01	89.0 ± 1.4	0.0007 ± 0.0001	0.098	79.6 ± 1.8	0.00123
Ta	0.04	111.4 ± 1.3	0.0003 ± 0.00005	0.03 ± 0.03	106.8 ± 2.5	0.00030 ± 0.00027	b.d.l	95.8 ± 1.5	
W	0.034	55.2 ± 1.3	0.0006	0.04	128.0 ± 3.3	0.0003	b.d.l	349.9 ± 7.9	
Pt	16.6 ± 0.5	10.5 ± 7.4	1.6 ± 1.1	9.9 ± 1.3	7.0 ± 0.2	1.4 ± 0.2	3.3 ± 2.5	6.6 ± 4.2	
Th	0.001	102.1 ± 0.8	0.00001	0.008	99.3 ± 2.8	0.00008	0.0018	88.8 ± 1.3	0.00002
U	0.01	32.0 ± 1.6	0.0003 ± 0.00002	b.d.l	50 ± 1.9		b.d.l	64.7 ± 0.7	

Table 4 continued

Composition	sp4			sp4			sp4		
Sample	Sp4_13			sp4_02			sp4_03		
T (°C)	1320			1300			1250		
Log fO_2	−4			−8			−8		
ΔQFM	3.0			−0.8			−0.3		
	Spinel	Glass	D_{sp}	Spinel	Glass	D_{sp}	Spinel	Glass	D_{sp}
n	2	5	2	6	5	6	4	3	4
Si	754	196259 ± 3263	0.004	1345 ± 193	200715 ± 9681	0.007 ± 0.001	493 ± 132	188962 ± 17043	0.0026 ± 0.0004
Ca	b.d.l	154283		1126 ± 413	157413	0.007 ± 0.003	789 ± 32	156184 ± 0.01	0.005
Sc	0.94 ± 0.35	23.7 ± 0.3	0.039 ± 0.015	1.3 ± 0.3	22.7 ± 0.8	0.06 ± 0.01	0.79 ± 0.03	23.7 ± 1.3	0.033 ± 0.007
Ti	888 ± 23	12824 ± 293	0.069 ± 0.002	1049 ± 45	13146 ± 316	0.080 ± 0.004	967 ± 14	13183 ± 611	0.073 ± 0.004
V	0.8 ± 0.2	23 ± 0.8	0.033 ± 0.007	53.7 ± 3.3	23.5 ± 1.7	2.3 ± 0.2	39.4 ± 0.8	22.4 ± 0.6	1.8
Cr	21197 ± 1549	107 ± 3.9	198 ± 16	8019 ± 1945	203 ± 173	40 ± 35	8094 ± 2038	157.9 ± 16.5	51.3 ± 5.4
Mn	22.1 ± 1.7	43.6 ± 0.4	0.51 ± 0.04	22.0 ± 2.9	44.5 ± 1.9	0.49 ± 0.07	19.6 ± 0.7	39.8 ± 0.8	0.49 ± 0.03
Co	66.9 ± 0.4	22.2 ± 0.6	3.01 ± 0.09	11.3 ± 1.2	3.5 ± 0.2	3.20 ± 0.40	57.6 ± 2.4	16.6 ± 1.7	3.5 ± 0.4
Ni	192 ± 10	22.6 ± 3.9	8.5 ± 1.5	b.d.l	15		158 ± 8	12.4 ± 7.4	12.78 ± 7.7
Cu	7.8 ± 0.3	71.7 ± 1.8	0.109 ± 0.005	b.d.l	7.7 ± 0.4		0.19	b.d.l	
Zn	nd	nd	nd	nd	nd	nd	nd	nd	nd
Ga	116.1 ± 0.8	22.2 ± 0.4	5.2 ± 0.10	19.5 ± 2.3	5.3 ± 0.4	3.65 ± 0.50	50.4 ± 2.5	7.6 ± 1.3	6.7 ± 1.2
Y	b.d.l	97 ± 0.5		b.d.l	91.1 ± 2.5		b.d.l	95.3 ± 6.1	
Zr	0.11	114.4 ± 2.9	0.0010	b.d.l	109.9 ± 3.2		0.05 ± 0.01	113.3 ± 4.9	0.00042 ± 0.00008
Nb	0.04	103.1 ± 2.4	0.0004	0.09 ± 0.05	105.9 ± 3.0	0.0008 ± 0.0005	0.02	105.7 ± 3.0	
Mo	b.d.l	162.6 ± 3.9		0.21 ± 0.16	25.7 ± 1.2	0.008 ± 0.006	0.17 ± 0.02	76.4 ± 0.03	0.0023 ± 0.0003
Rh	34.6 ± 4.2	0.36 ± 0.16	97 ± 46	1.1 ± 0.5	0.55 ± 0.11	2.0 ± 1.0	1.6 ± 0.4	0.84 ± 0.49	1.9 ± 1.7
Lu	0.044	83.9 ± 2.0	0.0005	0.020 ± 0.008	80.7 ± 3.2	0.0003 ± 0.0001	0.014 ± 0.005	85.7 ± 2.0	0.0002 ± 0.0001
Hf	0.098	79.6 ± 1.8	0.0012	0.11 ± 0.02	80.3 ± 3.3	0.0013 ± 0.0003	0.067 ± 0.013	82.5 ± 1.4	0.0008 ± 0.0003
Ta	b.d.l	95.8 ± 1.5		0.04 ± 0.03	103.7 ± 4.3	0.0003 ± 0.0002	0.030 ± 0.005	99.2 ± 3.2	0.0003
W	b.d.l	349.9 ± 7.9		0.03	109.9 ± 2.6	0.0003 ± 0.00001	b.d.l	111.0 ± 4.5	
Pt	3.3 ± 2.5	6.6 ± 4.2		16.4 ± 5.7	8.3 ± 1.4	1.98 ± 0.76	16.5 ± 2.8	13.9 ± 1.2	1.19 ± 0.11
Th	0.0018	88.8 ± 1.3	0.00002	0.005	94.8 ± 2.9	0.0001	b.d.l	91.6 ± 5.8	
U	b.d.l	64.7 ± 0.7		0.02	91.8 ± 0.7	0.00019	0.0003 ± 0.0002	85.1 ± 0.4	0.000004

Table 4 continued

Composition	sp4			sp4			sp5		
Sample	sp4_18			sp4_19			sp5_02		
T (°C)	1300			1300			1250		
Log fO_2	−0.7			−10			−8		
ΔQFM	6.5			−2.8			−0.3		
	Spinel	Glass	D_{sp}	Spinel	Glass	D_{sp}	Spinel	Glass	D_{sp}
n	5	5	5	4	5	4	6	5	6
Si	1156 ± 265	201084 ± 7604	0.006 ± 0.001	1418 ± 91	202538 ± 6937	0.007 ± 0.0005	331 ± 210	193038 ± 3860	0.0017 ± 0.001
Ca	790 ± 266	156634	0.005 ± 0.002	796 ± 311	155619 ± 0.01	0.005 ± 0.002	825 ± 237	148436 ± 0.01	0.006
Sc	1.3 ± 0.3	23.4 ± 0.7	0.05 ± 0.01	1.1 ± 0.2	22.7 ± 0.9	0.048 ± 0.009	0.74 ± 0.31	14.3 ± 0.1	0.05 ± 0.02
Ti	1014 ± 36	13140 ± 200	0.077 ± 0.003	1018 ± 16	13188 ± 31	0.077 ± 0.001	1197 ± 54	12989 ± 169	0.092 ± 0.004
V	b.d.l	22.9 ± 0.4		67.0 ± 5.9	12 ± 1.4	5.6 ± 0.8	49.3 ± 2.7	24.6 ± 0.7	2.0 ± 0.1
Cr	89 ± 19	4.3 ± 3.1	20.7 ± 15.5	4146 ± 584	94.3 ± 91.2	44.0 ± 43.0	8390 ± 1461	161.5 ± 124.9	52 ± 41
Mn	34.0 ± 4.4	48.2 ± 1.5	0.71 ± 0.09	17.5 ± 1.7	30.5 ± 1.0	0.57 ± 0.06	59.2 ± 2.1	104.7 ± 1.6	0.57 ± 0.02
Co	75.2 ± 3.4	23.3 ± 1.2	3.2 ± 0.2	1.0 ± 0.5	0.3	3.5 ± 1.8	75.5 ± 2.6	20.4 ± 0.6	3.7 ± 0.2
Ni	319 ± 39	39.8 ± 5.5	8.0 ± 1.5	b.d.l	b.d.l		151 ± 30	18.4 ± 0.2	8.2 ± 1.6
Cu	106.8 ± 6.0	304.6 ± 4.9	0.35 ± 0.02	b.d.l	2.7 ± 0.3		0.34	7.7 ± 0.1	0.04
Zn	177.5 ± 8.6	22.6 ± 3.0	7.9 ± 1.1	nd	nd	nd	nd	nd	nd
Ga	123.4 ± 4.3	25 ± 2.0	4.9 ± 0.4	0.7 ± 0.1	2.4 ± 0.1	0.27 ± 0.05	47.4 ± 2.5	7.5 ± 0.5	6.3 ± 0.6
Y	b.d.l	92.9 ± 2.4		b.d.l	91.4 ± 5.0		0.02	95.4 ± 1.0	0.0002
Zr	b.d.l	113 ± 2.1		0.27 ± 0.13	111.3 ± 1.7	0.002 ± 0.001	0.05	116.1 ± 0.6	0.0004
Nb	b.d.l	106.6 ± 2.3		0.08	101.4 ± 2.3	0.0007	0.02 ± 0.01	103.2 ± 2.5	0.0002 ± 0.0001
Mo	0.05	7.6 ± 0.5	0.007	0.23 ± 0.04	0.20 ± 0.10	1.02 ± 0.31	0.07 ± 0.03	62.2 ± 2.2	0.0011 ± 0.0006
Rh	986 ± 470	b.d.l		0.4 ± 0.1	0.32 ± 0.11	1.12 ± 0.42	0.04 ± 0.01	0.86 ± 0.16	0.051 ± 0.016
Lu	b.d.l	83.4 ± 2.6		0.037 ± 0.029	83.9 ± 3.8	0.00044 ± 0.00035	0.024 ± 0.007	86.3 ± 1.8	0.00028 ± 0.00008
Hf	0.069 ± 0.051	80.8 ± 1.5	0.0009 ± 0.0006	0.099 ± 0.049	78.6 ± 2.1	0.0013 ± 0.0006	0.08 ± 0.01	83.0 ± 2.3	0.001 ± 0.0001
Ta	0.020 ± 0.002	106.1 ± 2.2	0.00019 ± 0.00002	0.017 ± 0.005	103.3 ± 3.4	0.00017 ± 0.00005	0.026 ± 0.009	99.0 ± 3.4	0.00027 ± 0.00009
W	b.d.l	77.2 ± 3.5		b.d.l	18.7 ± 1.1		0.02 ± 0.01	107.1 ± 3.5	0.00018
Pt	20.7 ± 1.0	9.2 ± 0.2	2.26 ± 0.13	7.1 ± 2.0	4.9 ± 1.5	1.4 ± 0.6	0.1	8.7 ± 1.9	0.014
Th	b.d.l	93.9 ± 2.5		b.d.l	92.9 ± 2.9		0.0012	91.1 ± 3.7	0.00001
U	0.0012	48.9 ± 1.4	0.00002 ± 0.000001	0.002	93.5 ± 2.9	0.00002 ± 0.000001	0.0023 ± 0.0019	90.4 ± 3.8	0.00003 ± 0.00002

Table 4 continued

Composition	sp5			sp5			sp5		
Sample	sp5_03			sp5_05			sp5_10		
T (°C)	1220			1250			1220		
Log fO_2	−8			−8			−10		
ΔQFM	0.1			−0.3			−1.9		
	Spinel	Glass	D_{sp}	Spinel	Glass	D_{sp}	Spinel	Glass	D_{sp}
n	5	5	5	3	5	3	4	5	4
Si	530 ± 176	196397 ± 3935	0.0027 ± 0.0009	625 ± 81	205122 ± 3638	0.0030 ± 0.0004	627 ± 188	197920 ± 8723	0.003 ± 0.001
Ca	1023 ± 141	150359	0.0068 ± 0.0009	1056 ± 64	148794	0.0071 ± 0.0004	1412 ± 294	163038	0.009
Sc	0.61 ± 0.10	14.4 ± 0.3	0.042 ± 0.007	0.6 ± 0.08	14.9 ± 0.4	0.040 ± 0.006	0.81 ± 0.55	19.3 ± 0.7	0.04 ± 0.03
Ti	1252 ± 58	12971 ± 198	0.097 ± 0.005	1117 ± 23	13042 ± 167	0.086 ± 0.002	1675 ± 68	17706 ± 429	0.095 ± 0.004
V	40.5 ± 2.9	24 ± 0.4	1.7 ± 0.1	121.9 ± 3.2	22.6 ± 0.3	5.4 ± 0.2	134.6 ± 7.1	29.5 ± 0.2	4.6 ± 0.2
Cr	4008 ± 1543	61 ± 54	65 ± 63	7545 ± 1630	19.3 ± 0.6	391 ± 85	11087 ± 1756	49.2 ± 1.4	225 ± 36
Mn	59.0 ± 3.1	108.2 ± 3.5	0.55 ± 0.03	53.9 ± 1	103.3 ± 2.0	0.52 ± 0.01	54.2 ± 5.1	123.5 ± 2.0	0.44 ± 0.04
Co	89.6 ± 5.7	24 ± 2.3	3.7 ± 0.4	44.3 ± 1.9	12.4 ± 0.2	3.6 ± 0.2	57.0 ± 11.2	12.8 ± 0.3	4.5 ± 0.9
Ni	386 ± 12	29.7 ± 2.0	13.0 ± 0.9	29 ± 11	12.9	2.3	47 ± 18	b.d.l	
Cu	0.25 ± 0.09	13 ± 0.5	0.019 ± 0.007	0.22	5.5 ± 2.9	0.04	b.d.l	3.8 ± 0.8	
Zn	nd	nd	nd	nd	nd	nd	nd	nd	nd
Ga	78.6 ± 6.9	9.8 ± 0.7	7.98 ± 0.90	1.7 ± 0.3	0.8	2.0 ± 0.3	5.1 ± 1.7	1 ± 0.1	4.9 ± 1.7
Y	b.d.l	96.3 ± 0.9		0.04	98.8 ± 1.4	0.0004	b.d.l	131.7 ± 4.8	
Zr	0.05	116.5 ± 1.7	0.00045 ± 0.00002	0.14 ± 0.03	120.1 ± 1.9	0.0011 ± 0.0002	0.12 ± 0.07	163.8 ± 2.7	0.0007 ± 0.0004
Nb	0.01	104.9 ± 1.5	0.0001 ± 0.00002	0.05 ± 0.04	102.4 ± 2.4	0.0005 ± 0.0004	0.04	140.9 ± 1.6	0.00026 ± 0.00002
Mo	0.09 ± 0.02	124.5 ± 1.8	0.0008 ± 0.0002	0.31 ± 0.01	41.8 ± 1.3	0.0075 ± 0.0004	0.46 ± 0.11	101.5 ± 1.7	0.004 ± 0.001
Rh	0.03 ± 0.01	0.8 ± 0.3	0.037 ± 0.016	b.d.l	0.84 ± 0.30		0.04 ± 0.02	0.18 ± 0.06	0.24 ± 0.14
Lu	0.020 ± 0.004	83.8 ± 2.7	0.0002 ± 0.00004	0.03 ± 0.01	90.1 ± 2.1	0.0003 ± 0.0001	0.027 ± 0.009	122.2 ± 1.9	0.00022 ± 0.00007
Hf	0.061 ± 0.004	80.3 ± 1.9	0.0008 ± 0.00005	0.10 ± 0.03	85.9 ± 2.1	0.0011 ± 0.0004	0.081 ± 0.005	114 ± 1.0	0.00071 ± 0.00004
Ta	0.028 ± 0.003	95.4 ± 2.4	0.0003 ± 0.00003	0.06 ± 0.02	105.6 ± 1.4	0.0006 ± 0.0002	0.05 ± 0.02	130.7 ± 1.7	0.0004 ± 0.0002
W	0.006 ± 0.003	107.4 ± 4.3	0.00006 ± 0.00003	0.11 ± 0.10	336 ± 11	0.00034 ± 0.00029	b.d.l	542 ± 15	
Pt	0.8	8.7 ± 4.3	0.10	0.1	9.3 ± 1.8	0.014	0.4 ± 0.2	2.7 ± 0.6	0.14 ± 0.10
Th	0.0013 ± 0.0011	88.1 ± 2.5	0.000015 ± 0.000013	0.041 ± 0.029	94.5 ± 1.8	0.0004 ± 0.0003	0.013 ± 0.012	127 ± 3.9	0.00010 ± 0.00009
U	0.0019	86.4 ± 2.0	0.000022 ± 0.000001	0.030 ± 0.019	90.7 ± 2.1	0.0003 ± 0.0002	0.0023 ± 0.0015	120.1 ± 1.0	0.00002 ± 0.00001

Table 4 continued

Composition	sp5			sp5			sp6		
Sample	sp5_08			sp5_07			sp6_08		
T (°C)	1250			1220			1220		
Log fO_2	−12			−12			−6		
ΔQFM	−4.3			−3.9			2.1		
	Spinel	Glass	D_{sp}	Spinel	Glass	D_{sp}	Spinel	Glass	D_{sp}
n	6	5	5	2	5		3	5	3
Si	1052 ± 299	189270 ± 4718	0.006 ± 0.002	3039	191375 ± 5297	0.016	520 ± 373	179853 ± 8626	0.003 ± 0.002
Ca	1941 ± 402	152074	0.013 ± 0.003	b.d.l	166275		323	142161	0.002
Sc	0.67 ± 0.12	16.2 ± 0.4	0.041 ± 0.008	2.4	19.3 ± 0.6	0.12	11.8 ± 0.5	27.6 ± 0.7	0.43 ± 0.02
Ti	1459 ± 40	14188 ± 280	0.103 ± 0.003	1199 ± 14	17777 ± 678	0.067 ± 0.003	12762 ± 1056	13415 ± 191	0.95 ± 0.08
V	240 ± 21	24.8 ± 0.7	9.7 ± 0.9	215.8 ± 5.0	31.9 ± 0.6	6.8 ± 0.2	27.5 ± 2.6	26.7 ± 0.4	1.03 ± 0.10
Cr	6454 ± 473	73.7 ± 1.3	87.6 ± 6.6	8780 ± 3937	102.2 ± 4.9	86 ± 39	513 ± 127	1.3 ± 0.4	398 ± 159
Mn	56.9 ± 3.0	115.8 ± 2.8	0.49 ± 0.03	62.6 ± 4.8	131.2 ± 4.7	0.48 ± 0.04	155 ± 14	171.7 ± 7.8	0.90 ± 0.09
Co	11.8 ± 1.9	2.65 ± 0.08	4.5 ± 0.7	35.4 ± 0.8	5.3 ± 0.1	6.7 ± 0.2	88 ± 11	23.7 ± 0.3	3.7 ± 0.5
Ni	b.d.l	b.d.l		b.d.l	b.d.l		340 ± 25	20.3 ± 4.0	16.7 ± 3.5
Cu	0.30 ± 0.10	1.65 ± 0.07	0.18 ± 0.06	b.d.l	1.5 ± 0.1		3.4 ± 0.1	30.7 ± 0.8	0.109 ± 0.003
Zn	nd	nd	nd	nd	nd	nd	nd	nd	nd
Ga	0.66 ± 0.11	0.70 ± 0.10	0.94 ± 0.18	1.5	1.1 ± 0.3	1.4	66.6 ± 7.3	19 ± 0.4	3.5 ± 0.4
Y	0.34 ± 0.18	109.6 ± 3.3	0.003 ± 0.002	b.d.l	134 ± 2.0		0.13 ± 0.01	114.6 ± 4.2	0.0012 ± 0.0001
Zr	0.49 ± 0.24	134.9 ± 5.1	0.004 ± 0.002	b.d.l	161.3 ± 4.5		3.0 ± 0.2	137.7 ± 2.7	0.022 ± 0.001
Nb	0.72 ± 0.36	116.6 ± 2.7	0.006 ± 0.003	0.03	141.4 ± 3.8	0.00	0.96 ± 0.07	120 ± 3.3	0.0080 ± 0.0006
Mo	1.2 ± 0.3	8.3 ± 0.5	0.15 ± 0.04	1.9 ± 0.5	81.5 ± 5.3	0.023 ± 0.007	0.46 ± 0.11	163.5 ± 4.5	0.0028 ± 0.0006
Rh	0.01	0.52 ± 0.11	0.029	b.d.l	0.09 ± 0.04		2.4 ± 1.7	0.07 ± 0.05	34
Lu	0.33 ± 0.20	102.9 ± 4.4	0.003 ± 0.002	0.035	117.6 ± 1.6	0.0003	0.62 ± 0.03	97.1 ± 2.2	0.0064 ± 0.0003
Hf	0.36 ± 0.23	97.5 ± 2.0	0.004 ± 0.002	0.08 ± 0.02	116.2 ± 2.1	0.0007 ± 0.0001	4.0 ± 0.6	95.1 ± 1.9	0.042 ± 0.006
Ta	0.76 ± 0.40	116.3 ± 3.4	0.007 ± 0.003	0.03	138.7 ± 2.7	0.00022	2.0 ± 0.2	113.8 ± 4.7	0.017 ± 0.002
W	0.90 ± 0.45	163.2 ± 8.1	0.005 ± 0.003	0.028	499 ± 10	0.00006	0.19 ± 0.14	775 ± 58	0.0002
Pt	0.10 ± 0.02	5.6 ± 1.7	0.018 ± 0.007	b.d.l	1.3 ± 0.4		b.d.l	1.5 ± 0.7	
Th	0.46 ± 0.29	105.9 ± 5.1	0.004 ± 0.003	0.019	124.8 ± 2.3	0.00015	0.0037 ± 0.0017	103.1 ± 5.5	0.00004 ± 0.00002
U	0.62 ± 0.35	102.1 ± 3.6	0.006 ± 0.003	0.0032 ± 0.0007	123.3 ± 1.9	0.00003 ± 0.00001	0.010 ± 0.003	100.3 ± 4.3	0.00010 ± 0.00003

Table 4 continued

Composition	sp6			sp6			sp6		
Sample	sp6_03			sp6_04			sp6_09		
T (°C)	1220			1220			1220		
Log fO_2	−8			−10			−10		
ΔQFM	0.1			−1.9			−1.9		
	Spinel	Glass	D_{sp}	Spinel	Glass	D_{sp}	Spinel	Glass	D_{sp}
n	3	5	3	2	3	2	3	3	3
Si	507 ± 104	182308 ± 5906	0.0028 ± 0.0006	694 ± 320	170391 ± 10234	0.004 ± 0.002	410 ± 190	173479 ± 11452	0.002 ± 0.001
Ca	766 ± 121	141575	0.0054 ± 0.0009	923 ± 441	139267	0.007 ± 0.003	741 ± 54	140110	0.005
Sc	1.84 ± 0.06	25.5 ± 0.2	0.072 ± 0.002	1.2 ± 0.3	26.2 ± 0.8	0.044 ± 0.011	1.7 ± 0.3	26.6 ± 0.4	0.063 ± 0.010
Ti	1648 ± 27	12842 ± 59	0.13 ± 0.002	1400 ± 185	11816 ± 288	0.12 ± 0.02	1718 ± 66	13389 ± 455	0.13 ± 0.007
V	50.2 ± 4.2	24.7 ± 0.9	2.03 ± 0.18	133.3 ± 4.8	20.1 ± 0.2	6.6 ± 0.3	156.7 ± 0.9	23 ± 0.5	6.80 ± 0.15
Cr	5792 ± 2716	b.d.l		11191 ± 3424	29.2 ± 5.8	383 ± 140	13024 ± 2235	21.1 ± 1.8	616 ± 118
Mn	106.4 ± 3.7	161.1 ± 2.1	0.66 ± 0.02	98.4 ± 9.0	138.2 ± 2.0	0.71 ± 0.07	110.8 ± 9.1	158.5 ± 3.6	0.70 ± 0.06
Co	95.9 ± 4.2	23 ± 1.5	4.2 ± 0.33	65.8 ± 0.9	15.00 ± 0.3	4.4 ± 0.1	70.9 ± 2.4	13 ± 0.5	5.44 ± 0.29
Ni	327 ± 32	23.6 ± 6	13.9 ± 3.8	71 ± 11	b.d.l		48 ± 12	b.d.l	
Cu	0.25 ± 0.02	11.3 ± 0.3	0.022 ± 0.002	b.d.l	3.5 ± 0.2		b.d.l	3.7 ± 0.2	
Zn	nd	nd	nd	nd	nd	nd	nd	nd	nd
Ga	78.8 ± 2.5	10.3 ± 0.6	7.68 ± 0.49	12.4 ± 1.8	1.1 ± 0.1	11.3 ± 1.8	7.2 ± 1.0	1.1	6.8 ± 1.0
Y	b.d.l	105.8 ± 1.3		b.d.l	110.1 ± 3.8		0.02	112.4 ± 3	0.0001
Zr	0.08 ± 0.01	128.5 ± 1.3	0.00061 ± 0.00008	0.08	129.9 ± 4.1	0.0006	0.06 ± 0.01	135 ± 4	0.00045 ± 0.00009
Nb	0.03 ± 0.01	112 ± 1	0.00026 ± 0.00009	0.024 ± 0.008	102.7 ± 1.5	0.00024 ± 0.00008	0.03 ± 0.02	113.9 ± 1.9	0.0003 ± 0.0001
Mo	0.20 ± 0.03	113.8 ± 4.1	0.00173 ± 0.00031	0.73 ± 0.04	63.1 ± 0.5	0.0115 ± 0.0006	0.79 ± 0.04	71 ± 0.9	0.0111 ± 0.0005
Rh	0.19 ± 0.13	0.83 ± 0.57	0.23 ± 0.22	b.d.l	1.98 ± 0.21		b.d.l	0.54 ± 0.28	b.d.l
Lu	0.038 ± 0.006	90.1 ± 1.7	0.00043 ± 0.00007	0.026 ± 0.009	93.5 ± 2.3	0.00028 ± 0.00009	0.042 ± 0.001	97.2 ± 3.1	0.00043 ± 0.00002
Hf	0.134 ± 0.007	87.3 ± 2	0.00154 ± 0.00009	0.087 ± 0.045	91.0 ± 1.4	0.0010 ± 0.0005	0.13 ± 0.02	94.3 ± 3.7	0.0014 ± 0.0002
Ta	0.041 ± 0.005	105 ± 3.3	0.00039 ± 0.00005	0.037	107.1 ± 1.9	0.0003	0.045 ± 0.015	112.1 ± 2.4	0.0004 ± 0.0001
W	0.007 ± 0.006	106.4 ± 3.9	0.00007 ± 0.00006	0.017	2689 ± 72	0.000006	b.d.l	335.5 ± 11.6	b.d.l
Pt	0.60 ± 0.38	4.6 ± 3.0	0.13 ± 0.12	b.d.l	10.3 ± 0.8		0.1	2.1 ± 0.7	0.0328
Th	0.004	95.1 ± 2.9	0.00004	b.d.l	97.8 ± 4.8		0.0024	101.1 ± 4.3	0.00002
U	0.0092 ± 0.0007	90 ± 2	0.0001 ± 0.00001	b.d.l	81.7 ± 1.4		b.d.l	94.4 ± 4.1	b.d.l

Table 4 continued

Composition	sp6			sp6			sp12		
Sample	sp6_06			sp6_07			sp12_01		
T (°C)	1200			1220			1350		
Log fO_2	−10			−12			−8		
ΔQFM	−1.7			−3.9			−1.3		
	Spinel	Glass	D_{sp}	Spinel	Glass	D_{sp}	Spinel	Glass	D_{sp}
n	5	5	5	1	5	1	1	5	2
Si	323 ± 65	183296 ± 4721	0.0018 ± 0.0004	b.d.l	178994 ± 5239		b.d.l	202303 ± 5852	b.d.l
Ca	659 ± 170	140039	0.005 ± 0.001	b.d.l	139045		b.d.l	153569	b.d.l
Sc	1.65 ± 0.10	28 ± 0.4	0.059 ± 0.003	2.23	27.5 ± 0.4	0.08	b.d.l	24.3 ± 0.4	b.d.l
Ti	1444 ± 60	12935 ± 314	0.11 ± 0.005	1834	13570 ± 143	0.14	1159	13084 ± 182	0.089
V	137.1 ± 8.1	21.8 ± 0.6	6.3 ± 0.4	284.5	26.3 ± 0.8	10.8	74.8	21.9 ± 0.5	3.4
Cr	6571 ± 3769	8.6 ± 6.2	761 ± 701	11630	67.6 ± 4.4	172	45841	428.4 ± 30.7	107
Mn	95.7 ± 2.6	154.8 ± 3.9	0.62 ± 0.02	109.6	169.3 ± 4.8	0.65	8.1	40.8 ± 1.1	0.20
Co	72.2 ± 5.8	14.9 ± 0.3	4.9 ± 0.4	23	4.2 ± 0.1	5.5	5	2 ± 0.1	2.45
Ni	74 ± 12	b.d.l		b.d.l	b.d.l		b.d.l	b.d.l	b.d.l
Cu	b.d.l	3.8 ± 0.1		b.d.l	1.3		6.11	8.3 ± 1.4	0.74
Zn	nd	nd	nd	nd	nd	nd	nd	nd	nd
Ga	11.3 ± 3.3	1.1 ± 0.1	10.1 ± 3.0	0.9	0.8 ± 0.1	1.2	4.6	1.5 ± 0.2	3.0
Y	0.01	117.9 ± 2.7	0.00010	b.d.l	113.7 ± 1.2		b.d.l	98.4 ± 2.1	
Zr	0.07 ± 0.02	137.8 ± 2.9	0.00049 ± 0.00016	0.10	135.5 ± 1.6	0.0007	0.25	115.4 ± 0.7	0.002
Nb	0.01	111.5 ± 0.8	0.00012 ± 0.00004	0.04	118.0 ± 2.6	0.0004	b.d.l	103.6 ± 0.7	
Mo	0.57 ± 0.17	57.9 ± 2.3	0.0099 ± 0.0029	3.4	39.9 ± 1.9	0.085	b.d.l	22.1 ± 3.9	
Rh	b.d.l	0.94 ± 0.29	0.048 ± 0.015	b.d.l	0.08 ± 0.05		0.6	0.37 ± 0.13	1.5
Lu	0.029 ± 0.005	98 ± 1.0	0.00030 ± 0.00005	b.d.l	99.4 ± 2.3		0.14	86.2 ± 1.1	0.0016
Hf	0.095 ± 0.021	92.9 ± 1.6	0.0010 ± 0.0002	0.11	98.2 ± 2.4	0.0011	0.33	81.1 ± 1.4	0.0041
Ta	0.033 ± 0.008	113.1 ± 1.2	0.00029 ± 0.00007	0.04	118.3 ± 1.7	0.0003	0.072	98.5 ± 0.8	0.00073
W	b.d.l	1656 ± 101		b.d.l	187.1 ± 1.6		b.d.l	189.9 ± 5.2	
Pt	b.d.l	3.7 ± 2.4	0.035 ± 0.029	b.d.l	0.7 ± 0.4		2.5	6.0 ± 0.7	0.41
Th	0.0021	103.5 ± 1.3	0.00002	b.d.l	106.2 ± 0.8		0.023	91.6 ± 1.8	0.0003
U	0.0008 ± 0.0007	90.7 ± 2	0.000009 ± 0.000008	b.d.l	100.1 ± 0.5		b.d.l	85.9 ± 0.9	

Table 4 continued

Composition	sp12			sp12			sp10		
Sample	sp12_02a			sp12_02b			sp10_02		
T (°C)	1320			1320			1430		
Log fO_2	−4			−4			−4		
ΔQFM	3.0			3.0			2.1		
	Spinel	Glass	D_{sp}	Spinel	Glass	D_{sp}	Spinel	Glass	D_{sp}
n	1	4	3	5	5	5	3	5	3
Si	b.d.l	194230 ± 5837		b.l.d	203146 ± 3036		2260	190814 ± 7789	0.012
Ca	b.d.l	156315		619	156173 ± 318	0.0040	669	150087	0.004
Sc	1.97	23.9 ± 0.8	0.082	b.l.d	24 ± 0.7		7.6 ± 6.2	110.8 ± 2.8	0.068 ± 0.056
Ti	1010	13415 ± 276	0.075	1059 ± 35	13420 ± 236	0.079 ± 0.003	33 ± 18	508 ± 10	0.065 ± 0.035
V	b.d.l	23 ± 0.5		0.9 ± 0.3	23.4 ± 0.5	0.038 ± 0.011	97.1 ± 29.7	123.7 ± 2.4	0.78 ± 0.24
Cr	42495	189.1 ± 9.3	225	45345 ± 2160	167 ± 4.7	272 ± 15	83933 ± 41645	1002 ± 25	84 ± 42
Mn	26	44.2 ± 0.7	0.58	28.1 ± 0.8	44.4 ± 1.2	0.63 ± 0.02	35.6 ± 15	100 ± 1.3	0.36 ± 0.15
Co	93	21.7 ± 0.3	4.3	78.7 ± 5.9	21.5 ± 0.5	3.7 ± 0.3	29.3 ± 11.6	18 ± 0.4	1.6 ± 0.6
Ni	288	19.1 ± 6.1	15	271 ± 71	17.4 ± 1.4	15.5 ± 4.3	b.d.l	b.d.l	
Cu	19	148.4 ± 5.3	0.13	15.7 ± 1.4	151 ± 1.4	0.104 ± 0.009	b.d.l	26 ± 0.7	
Zn	nd	nd	nd	nd	nd	nd	nd	nd	nd
Ga	141	28.4 ± 0.6	5.0	152 ± 13	30.5 ± 1.1	5.0 ± 0.5	22.8 ± 4.4	2.5 ± 0.2	9.2 ± 1.9
Y	b.d.l	97.5 ± 3.0		0.09	96.3 ± 3.3	0.0009	b.d.l	112.5 ± 1.6	
Zr	b.d.l	115.2 ± 3.9		b.d.l	114 ± 2.9		0.34 ± 0.25	116.5 ± 2	0.003 ± 0.002
Nb	0.06	106.9 ± 1.1	0.0005	0.06 ± 0.01	107 ± 1.9	0.00056 ± 0.00007	0.04	99.6 ± 1.4	0.0004
Mo	b.d.l	823 ± 17		0.06	774 ± 19	0.00008	b.d.l	11.4 ± 0.4	
Rh	75	0.18 ± 0.07	408	56 ± 12	0.18 ± 0.04	315 ± 95	b.d.l	12.7 ± 1.1	
Lu	0.037	86.0 ± 2.2	0.0004	0.071	85.2 ± 2.7	0.0008	0.065	90.1 ± 1.1	0.0007
Hf	0.21	83.3 ± 0.6	0.0025	0.073 ± 0.033	81.9 ± 1.8	0.0009 ± 0.0004	0.38 ± 0.22	82.2 ± 1.2	0.0046 ± 0.0026
Ta	b.d.l	101 ± 2.1		0.05	100.2 ± 1.8	0.0005	0.086	94.6 ± 1.1	0.00091
W	b.d.l	829 ± 11.6		0.031	945 ± 32	0.00003	0.182	4632.3 ± 87.7	0.00004
Pt	5.5	1.3 ± 0.7	4.1	b.d.l	2.3 ± 0.8		5.7 ± 5.1	16.4 ± 12.5	
Th	0.019	90.7 ± 3.1	0.0002	0.0038	91.3 ± 2.9	0.00004	b.d.l	90.7 ± 1.4	
U	0.009	62.6 ± 1.1	0.0001	0.0026 ± 0.0006	60.4 ± 1.5	0.00004 ± 0.00001	0.0049	59.1 ± 0.3	0.00008

Table 4 continued

Composition	sp14			sp15			sp2		
Sample	sp14_01			sp15_01			sp2_05		
T (°C)	1350			1350			1300		
Log fO_2	−8			−8			−0.7		
ΔQFM	−1.3			−1.3			6.5		
	Spinel	Glass	D_{sp}	Spinel	Glass	D_{sp}	Spinel	Glass	D_{sp}
n	3	5	3	4	5	4		3	
Si	860	181389 ± 1906	0.0047	b.d.l	179264 ± 9677		549	195900 ± 5579	0.0028
Ca	b.d.l	143548		546	137559 ± 0.01	0.0040	569 ± 60	154811 ± 608	0.0037
Sc	1.83	14.4 ± 0.2	0.13	3.4 ± 1.4	24.8 ± 0.9	0.14 ± 0.06	b.d.l	0.5 ± 0.1	
Ti	1799 ± 227	12505 ± 224	0.14 ± 0.02	2798 ± 576	12392 ± 151	0.23 ± 0.05	15 ± 1.0	244 ± 4.0	0.062 ± 0.0059
V	106 ± 19	21.3 ± 0.6	5.0 ± 0.9	106 ± 12	21.6 ± 0.7	4.9 ± 0.6	0.3	144.1 ± 2.8	0.0020
Cr	150444 ± 42921	558 ± 63	270 ± 83	159431 ± 7978	682 ± 34	234 ± 17	2840 ± 1143	27	105
Mn	65.9 ± 6.5	94.5 ± 1.9	0.70 ± 0.07	132 ± 35	147 ± 4.4	0.90 ± 0.24	b.d.l	b.d.l	
Co	62 ± 17	16.8 ± 0.2	3.7 ± 1.0	45.9 ± 8.2	13.9 ± 0.3	3.3 ± 0.6	287.2 ± 12.9	95.5 ± 3.9	3.0 ± 0.2
Ni	151	b.d.l		71	14.2 ± 2.9	5.0	b.d.l	b.d.l	
Cu	1.8 ± 1.3	10.5 ± 0.2	0.17 ± 0.12	b.d.l	11.8 ± 0.3		773 ± 108	2164 ± 154	0.36 ± 0.06
Zn	nd	nd	nd	nd	nd	nd	202	22.5	9.0
Ga	4.3 ± 0.9	1.3 ± 0.1	3.3 ± 0.7	5.6 ± 2.1	1.5	3.8 ± 1.4	468 ± 18	98.5 ± 5.7	4.8 ± 0.3
Y	0.26 ± 0.25	98.8 ± 0.6	0.0026 ± 0.0025	0.23 ± 0.21	104 ± 5.0	0.0022 ± 0.0021	b.d.l	b.d.l	
Zr	0.33 ± 0.07	118.8 ± 2.1	0.0027 ± 0.0006	0.68 ± 0.31	125 ± 6.3	0.0054 ± 0.0025	b.d.l	119.5 ± 5.9	
Nb	0.19 ± 0.10	102.2 ± 1.3	0.0018 ± 0.0009	0.15 ± 0.08	107 ± 2.0	0.0014 ± 0.00075	0.31	96.4 ± 5.0	0.0032
Mo	1.5 ± 1.1	160.5 ± 0.8	0.009 ± 0.007	2.7 ± 0.8	211 ± 2.7	0.013 ± 0.0038	b.d.l	b.d.l	
Rh	b.d.l	b.d.l		0.3	0.47 ± 0.33	0.72	b.d.l	b.d.l	
Lu	0.096 ± 0.075	89.6 ± 1.9	0.0011 ± 0.0008	0.13 ± 0.04	92.0 ± 4.4	0.0014 ± 0.0004	b.d.l	b.d.l	
Hf	0.36 ± 0.21	86.8 ± 1.8	0.004 ± 0.002	0.71 ± 0.24	90.2 ± 1.7	0.008 ± 0.003	0.17 ± 0.16	89.2 ± 2.7	0.0019 ± 0.0017
Ta	0.10 ± 0.05	104 ± 1.5	0.0010 ± 0.0005	0.19 ± 0.08	111 ± 1.8	0.0017 ± 0.0007	0.018	88.8 ± 2.9	0.0002
W	0.04 ± 0.02	377 ± 5.3	0.00011 ± 0.00005	0.33 ± 0.21	298 ± 13	0.0011 ± 0.0007	b.d.l	44.5 ± 1.9	
Pt	0.3	8.8 ± 3.9	0.037	b.d.l	11.3 ± 2.1		b.d.l	7.8 ± 1.0	
Th	0.003	93.3 ± 2.5	0.00003	0.024 ± 0.006	98.2 ± 4.8	0.00024 ± 0.00007	b.d.l	94.3 ± 3.8	
U	0.006 ± 0.004	84.0 ± 2.2	0.00007 ± 0.00004	b.d.l	87.2 ± 1.9		0.0055	9.9 ± 0.2	0.0006

Table 4 continued

Composition	prg			prg			prg		
Sample	prg11			prg12			prg13		
T (°C)	1300			1300			1300		
Log fO_2	−0.7			−0.7			−10		
ΔQFM	6.5			6.5			−2.8		
	Spinel	Glass	D_{sp}	Spinel	Glass	D_{sp}	Spinel	Glass	D_{sp}
n	7	5	7	7	5	7	5	5	5
Si	1185 ± 279	193874 ± 4536	0.006 ± 0.001	1251 ± 203	203211 ± 4252	0.006 ± 0.001	1012 ± 257	186119 ± 9464	0.005 ± 0.001
Ca	1059 ± 285	161844	0.007 ± 0.002	910 ± 297	161537	0.006 ± 0.002	1029 ± 225	160601	0.006
Sc	nd	nd	nd	nd	nd	nd	nd	nd	nd
Ti	1008 ± 43	13604 ± 210	0.074 ± 0.003	1000 ± 39	13679 ± 293	0.073 ± 0.003	1062 ± 23	13818 ± 183	0.077 ± 0.002
V	nd	nd	nd	nd	nd	nd	nd	nd	nd
Cr	nd	nd	nd	nd	nd	nd	nd	nd	nd
Mn	nd	nd	nd	nd	nd	nd	nd	nd	nd
Co	nd	nd	nd	nd	nd	nd	nd	nd	nd
Ni	nd	nd	nd	nd	nd	nd	nd	nd	nd
Cu	nd	nd	nd	nd	nd	nd	nd	nd	nd
Zn	nd	nd	nd	nd	nd	nd	nd	nd	nd
Ga	nd	nd	nd	nd	nd	nd	nd	nd	nd
Y	nd	nd	nd	nd	nd	nd	nd	nd	nd
Zr	nd	nd	nd	nd	nd	nd	nd	nd	nd
Nb	nd	nd	nd	nd	nd	nd	nd	nd	nd
Mo	nd	nd	nd	nd	nd	nd	nd	nd	nd
Rh	702 ± 242	19.0 ± 9.8	37 ± 23	4741 ± 1289	33 ± 17	144 ± 83	0.2 ± 0.1	0.09 ± 0.03	2.6 ± 1.2
Lu	nd	nd	nd	nd	nd	nd	nd	nd	nd
Hf	nd	nd	nd	nd	nd	nd	nd	nd	nd
Ta	nd	nd	nd	nd	nd	nd	nd	nd	nd
W	nd	nd	nd	nd	nd	nd	nd	nd	nd
Pt	21.3 ± 0.9	9.6 ± 0.5	2.2 ± 0.1	15.8 ± 4.5	8.0 ± 0.4	2.0 ± 0.6	9.9 ± 3.7	3.5 ± 1.6	2.8 ± 1.6
Th	nd	nd	nd	nd	nd	nd	nd	nd	nd
U	nd	nd	nd	nd	nd	nd	nd	nd	nd

Table 4 continued

Composition	prg		
Sample	prg14		
T (°C)	1300		
Log fO_2	−10		
ΔQFM	−2.8		
	Spinel	Glass	D_{sp}
n	7	5	7
Si	1165 ± 162	193040 ± 9507	0.0060 ± 0.0009
Ca	1039 ± 234	162180 ± 0	0.0064 ± 0.0014
Sc	nd	nd	nd
Ti	1068 ± 60	13875 ± 788	0.077 ± 0.006
V	nd	nd	nd
Cr	nd	nd	nd
Mn	nd	nd	nd
Co	nd	nd	nd
Ni	nd	nd	nd
Cu	nd	nd	nd
Zn	nd	nd	nd
Ga	nd	nd	nd
Y	nd	nd	nd
Zr	nd	nd	nd
Nb	nd	nd	nd
Mo	nd	nd	nd
Rh	1.1 ± 0.5	0.54 ± 0.2	2.1 ± 1.2
Lu	nd	nd	nd
Hf	nd	nd	nd
Ta	nd	nd	nd
W	nd	nd	nd
Pt	9.7 ± 4.3	3.8 ± 0.4	2.6 ± 1.2
Th	nd	nd	nd
U	nd	nd	nd

b.d.l. below detection limit, *nd* not done, these elements were not added to the experiment. Uncertainties are given as 1σ standard deviation

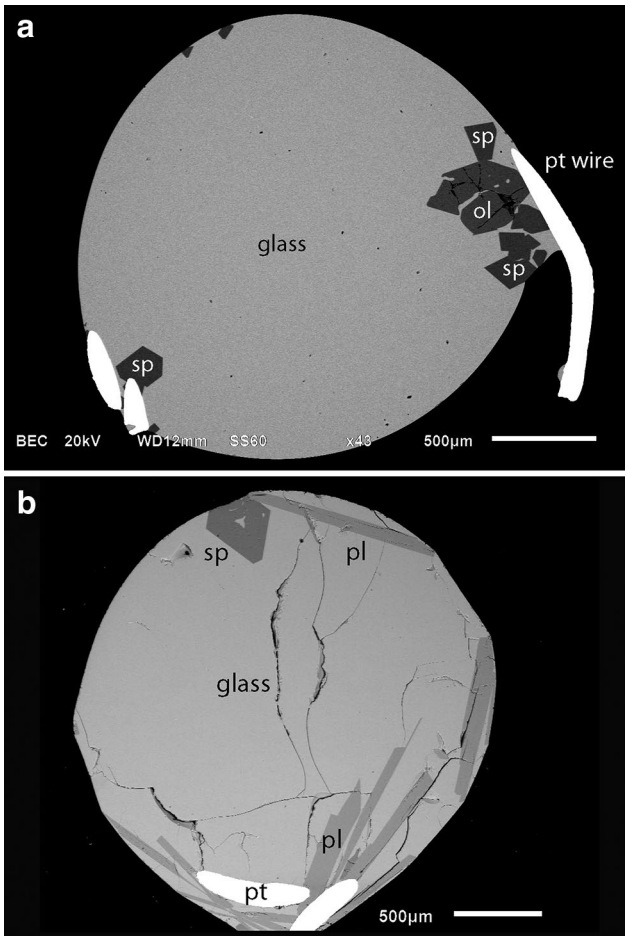

Fig. 1 SEM backscatter image of two typical run products. **a** sp2_05 contains spinel and olivine crystals, mostly close to the rim of the melt droplet or close to the noble metal wire. **b** sp5_08 contains one large spinel crystal with obvious melt inclusion, and several large plagioclase lathes

usually up to five spots in spinels. Whenever possible, we did core and rim analyses of spinels; however, due to the relatively small size of the crystals, this could not be done for every sample. The aim of the study was to investigate trace element partitioning for spinel; however, as some experiments contained other minerals (olivine and plagioclase), these were also measured. The data from cpx-bearing experiments is not shown, as these experiments appear to be not fully equilibrated for trace elements (see above).

The glasses are always homogeneous in terms of trace elements (Table 4). The spinels appear to be homogeneous in trace elements except in the case where there is obvious major element zonation in the crystal (sample sp6_08); in this case, only the rim measurements were used for calculating partition coefficients.

Plagioclase and olivine show no zonation in trace elements. Trace elements concentrations and partition coefficients for olivine and plagioclase are shown in table 7 of the electronic supplements, but are not discussed further. However, the plagioclase partition coefficients are in good agreement with the data from Aigner-Torres et al. (2007). Experimental partitioning data for olivine are widely available [see for example (Beattie 1994; Mallmann and O'Neill 2009; Nielsen et al. 1992)]; our olivine partitioning data are in good agreement with those publications.

Attainment of equilibrium

For an accurate determination of trace element partition coefficients, it is important to demonstrate that equilibrium between spinel and melt has been attained in the experiments. Three items of evidence strongly indicate equilibrium conditions: (1) Spinels as well as melt are very

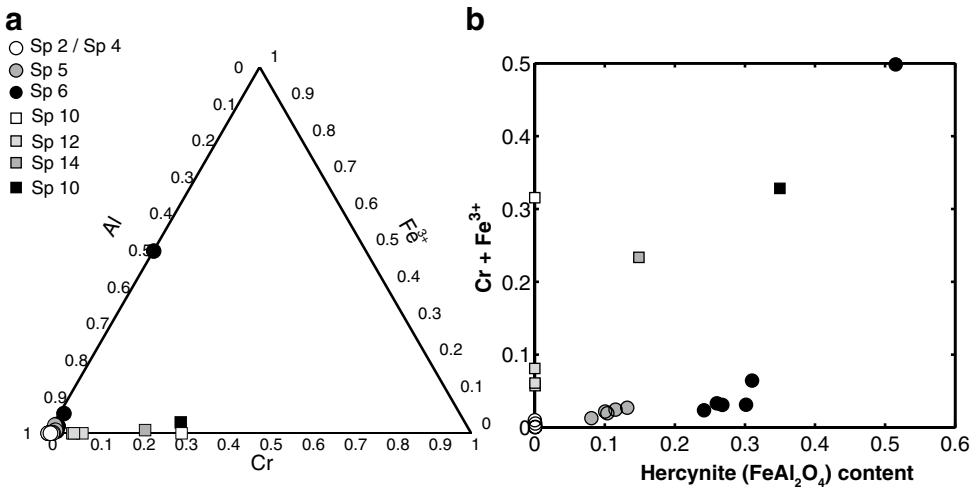

Fig. 2 Compositional variation of the spinel-structured oxides in our experiments. The ternary diagram (**a**) shows the compositional range on the octahedral (B) site: the Al–Cr–Fe^{3+} content of the spinel, which corresponds to the endmembers spinel, chromite and magnetite. **b** Compositional range on the tetrahedral (A) site (Mg–Fe), by plotting the hercynite ($FeAl_2O_4$) content against Cr + Fe^{3+} (normalized to 1: this can be seen as the total chromite + magnetite content)

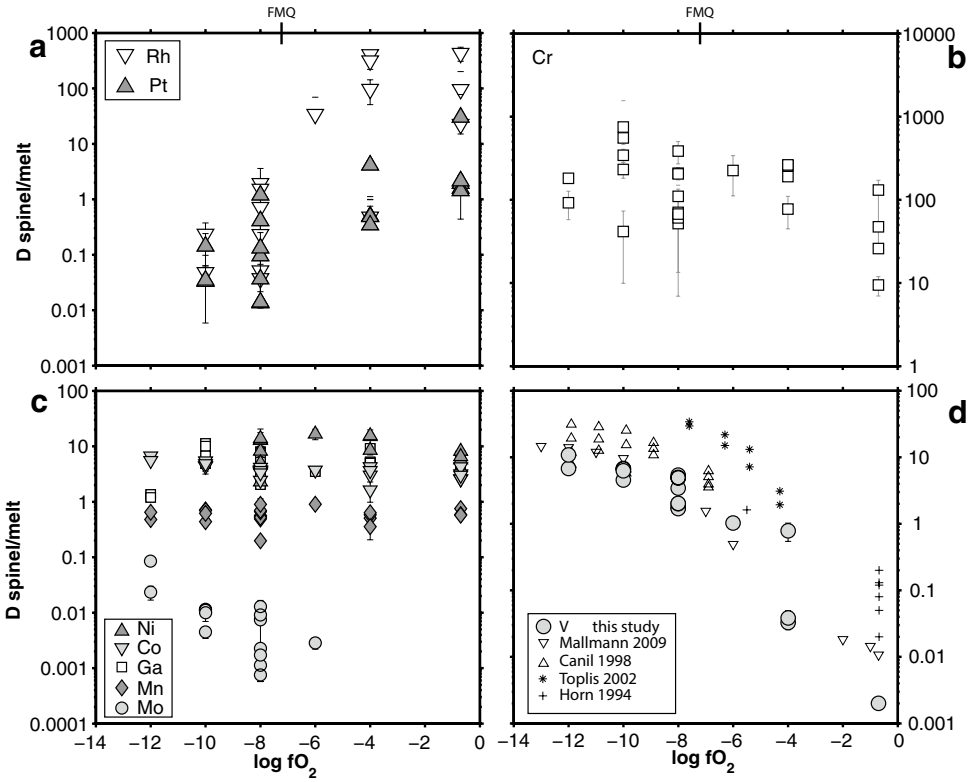

Fig. 3 Trace element partition coefficients of several elements plotted against fO_2. The *tickmark* shows the position of the quartz–fayalite–magnetite (QFM) buffer at 1300 °C. Our data show that Cr, Ni, Co and Ga are compatible in spinel. V partition coefficients range from compatible to incompatible, depending of fO_2. Vanadium partitioning data from (Canil 1999; Horn et al. 1994; Mallmann and O'Neill 2009; Toplis and Corgne 2002) are shown for comparison. Mo is always incompatible, but D_{Mo} varies with fO_2. The platinum group elements Pt and Rh show very variable partitioning, for details see text

homogeneous in each individual run. There is no evidence for zonation within spinel crystals or melt. (2) Spinels generally show euhedral habit; especially, all spinel–melt contacts are straight without resorbtion textures. (3) Despite significant differences in residual melt fractions between the different runs, all calculated spinel–melt trace element partition coefficients are internally consistent.

Bulk loss of trace elements

For a number of trace elements, bulk concentrations (calculated from mass balance) are lower than expected. Bulk loss of an element from the experimental charge can be caused by either volatile behavior of the element or by alloying with the Pt wire. In our experiments, Cd, Sn, Sb and Pb exhibit strong volatile behavior. Several other elements (Ni, Co, Ga, Zn, Cu, Cr) show bulk loss only with certain fO_2 conditions. Ni, Co and Ga concentrations are slightly lower in the experiments with the lowest oxygen fugacity ($fO_2 < -10$), but while Ga might be volatile, Ni and Co are most likely not. Furthermore, if the bulk element concentrations are only decreased at the lowest fO_2, this could indicate that the element is susceptible to alloying with the platinum wire. This is known to be the case for Fe and may also be the case for Ni, Co and Cu. Bulk loss of an element during the experiment poses a potential problem for determining partition coefficient. When crystals and melts equilibrate early during the experimental run and the concentration of the element in the melt subsequently decreases due to volatility, it is uncertain whether crystal–melt equilibrium is preserved. Zoning of the element in the crystals would be an indication for changing melt composition during the experimental run. If loss of an element occurred and the mineral is not zoned, this means that either the mineral re-equilibrated with the melt during the experimental run, in which case the partition coefficients is correct, or that the crystal formed early during the run and did not re-equilibrate at all with the new melt composition, in which case the calculated partition coefficient will overestimate the true partition coefficient. Therefore, the partition coefficients derived from these particular experiments need to be viewed with extreme care.

Partition coefficients

Partition coefficients were calculated from the trace element data according to Eq. (1). The partition coefficient of a certain element i is defined as the ratio of the concentration of the element in the crystal and the melt. If the element favors the crystal over the melt ($D_i > 1$), the element is called compatible; otherwise, it is incompatible ($D_i < 1$).

$$D_i = c^i_{mineral}/c^i_{melt} \quad (1)$$

Concentrations are in ppm.

Table 5 Fitting parameters for D_V and D_{Mo} (Eqs. 2, 3)

	a	b	c	d	R^2
V	−3.041	−0.6734	−0.02893	6.74E − 05	0.885
Mo	−4.449	−0.2486			0.637

According to Henry's law, the partition coefficient of a certain trace element is independent of the concentration of the trace element. This, however, only applies when the concentration of the element is sufficiently low. For spinel, it has been suggested that the concentration needs to be lower than 1 wt% for most elements (Horn et al. 1994). In our experiments, the trace element concentrations in the crystals are usually lower than 200 ppm, and we therefore assume that Henry's law is valid in our experiments.

Mineral–melt partition coefficients are not constants, but may depend on a number of factors, including pressure, temperature, oxygen fugacity and mineral and melt composition. The aim of this study is to constrain the trace element partitioning behavior as a function of spinel composition and oxygen fugacity. Although we performed experiments over a range of different temperatures, it is difficult to quantify the temperature effect, because the starting composition has a large effect on the position of the liquidus, and therefore, experiments with different compositions were performed by necessity at different temperature conditions. Thus, the Fe-rich experiments were performed at lower temperatures and the Cr-rich experiments under higher temperatures. In order to be able to disentangle the effect of composition from a temperature effect, some experiments were performed containing both Cr and Fe, at intermediate temperatures.

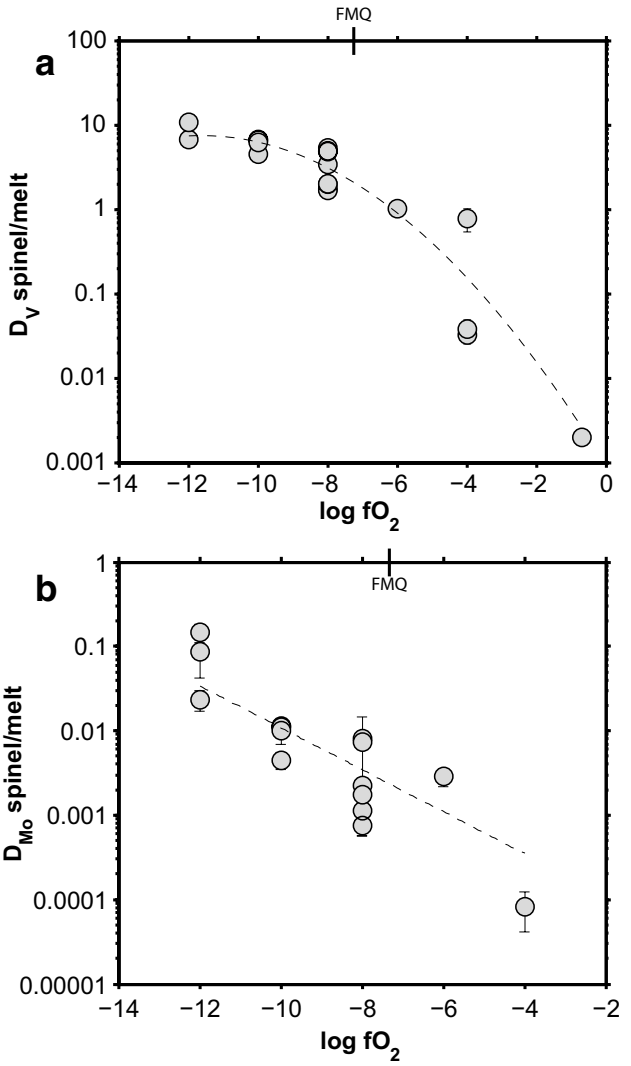

Fig. 4 Partition coefficients of V and Mo strongly depend on redox conditions. Depicted are D_V (**a**) and D_{Mo} (**b**) and non-limit fitting results according to Eqs. (2) and (3). The *tickmark* shows the position of the QFM buffer at 1300 °C

Discussion

Spinel trace element partitioning

Nickel and cobalt

Ni and Co show similar partitioning behavior, Ni being slightly more compatible than Co; D_{Co} values range from 1.6 to 6.7, and D_{Ni} values from 6.1 to 22. Both Ni and Co partition coefficients seem to decrease slightly with increasing oxygen fugacity, and they slightly decrease with increasing temperature. However, mass balance calculations indicate that bulk loss of both Ni and Co has occurred in the experiments with the lowest oxygen fugacity (log $fO_2 = -12$, see Table 3). For reasons explained above, this means that the partition coefficients could be overestimated for these runs (i.e., runs 8 and 9). This suggests that the decreasing trends could be an artifact for the experiments at low fO_2, and that D values are in fact quite constant. Furthermore, there is also no obvious effect of spinel composition. Overall, our D_{Ni} and D_{Co} values are in good agreement with the data by both Righter et al., (2006) and Horn et al. (1994). The decreasing of D_{Ni} and D_{Co} trend is also noted by Horn et al. (1994). However, as their experimental set up is similar to ours, their experiments might have been affected with the same issues of Ni and Co loss, possibly to the Pt wire.

Gallium

Gallium is compatible in spinel in most experiments, with uniform D values between 0.9 and 11.2, and with slightly lower D values in the most reducing experiments with an

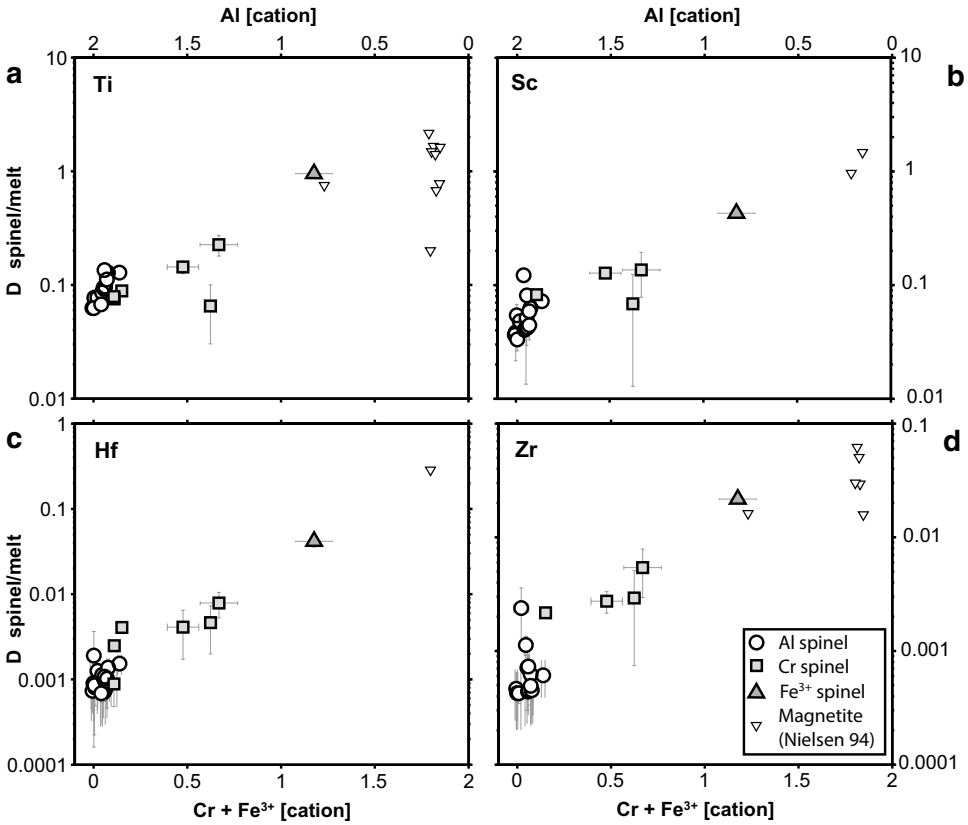

Fig. 5 D_{Ti}, D_{Sc}, D_{Zr} and D_{Hf} plotted against trivalent cation content of the spinel. The *different symbols* represent the Al-rich spinels, the Cr-containing spinels and de Fe^{3+}-containing spinels. Some selected partition coefficients for (Ti)-magnetite from (Nielsen et al. 1994) are also shown for comparison (selected for low (i.e., >2 wt %) TiO_2 concentrations)

oxygen fugacity of log −12. There is no significant effect of temperature or composition. Note that Ga loss has occurred in the experiments with low oxygen fugacity (log fO_2 < −8) or high temperatures (>1300 °C), indicating volatile behavior. However, this does not appear to have an effect on the partition coefficients, as they are quite constant except for the lowest fO_2, and if those experiments would be compromised due to volatility, we would expect the *D*'s to be higher rather than lower.

Chromium

Cr is highly compatible in spinel, with partition coefficients between 26 and 751. Due to its very high compatibility, in the experiments with the higher Cr concentrations (500–2000 ppm in the starting material), Cr becomes a major element in spinel, with concentrations up to 30 wt%. With such high concentrations, Henry's law does not apply (Horn et al. 1994). However, although they show some of scatter, the *D* values for these experiments fall in the same range as the ones with lower Cr concentrations. The partition coefficients are highest at intermediate oxygen fugacity (−10 < log fO_2 < −6) and slightly decrease at both high and at low oxygen fugacity. This is probably due to changes in valence state as Cr may occur as Cr^{2+}, Cr^{3+}, and Cr^{6+} under these experimental conditions. At low oxygen fugacity and high temperatures, a significant amount of Cr will occur as Cr^{2+}, while at high fO_2 Cr might occur partly as Cr^{6+} (Berry and O'Neill 2004). At intermediate fO_2, the *D* values are the highest, so the trivalent species of Cr appears to be the most compatible in spinel, which is to be expected considering the solid solution between spinel and (Mg-)chromite.

It is interesting to note that during experiments at higher temperatures (>1300 °C) and with the highest oxygen fugacities (experiments performed in air, or CO_2 and >1400 °C), Cr was lost quantitatively from the experimental charge, suggesting high volatility under these conditions. We assume that it is only the hexavalent species of Cr that shows volatile behavior in these runs, because in the more reducing experiments where only Cr^{3+} and Cr^{2+} are stable, there is no volatile loss. If Cr is lost during those experiments, this implies that the calculated partition coefficients are indeed overestimated. Since Cr diffusion is known to be slow (Ganguly et al. 2007), the spinel is not expected to re-equilibrate with the melt. This is evident from some experiments that suffered from Cr loss, where lots of small (<5 μm across) spinels are heavily zoned in Cr–Al, with a Cr-rich core and a Cr-poor rim, and low Cr concentrations in the glasses. This would explain the relatively large spread of *D* values at a log fO_2 of −0.7 and suggest that only the lowest *D* values are correct for these oxidizing conditions.

Vanadium

Vanadium partitioning in spinel is strongly controlled by oxygen fugacity, V changes from incompatible at oxidizing conditions (0.002 at log fO_2 of −0.7, 0.033 at log fO_2 of −6) to compatible at reducing conditions (10.8 at a log fO_2 of −12). The partitioning of V between melts and spinel and other minerals has been studied extensively (Canil 1999; Mallmann and O'Neill 2009; Righter et al. 2006; Toplis and Corgne 2002). Because V can occur in several valence states (V^{3+}, V^{4+} and V^{5+}) in oxygen fugacities relevant to the Earth and related planetary bodies, it has been suggested that V could be a powerful indicator for redox states of magmas (Canil 1999; Lee et al. 2005; Mallmann and O'Neill 2009, 2013). When comparing our data to literature values, our data shows a more gradual trend when compared with the data of Canil (1999) and Righter et al. (2006), and the actual D_V values are somewhat lower (see Fig. 3d). However, our data are in good agreement with recent results by Mallmann and O'Neill (2009). The discrepancy between early datasets and our data may be explained by spinel composition, as spinels in the experiments by Canil are characterized by very high V contents. Experiments by Righter (2006) and Toplis (2002) contain mainly (Ti-)magnetite-rich spinels compared to more Al-rich spinels in our and Mallmann and O'Neill's studies. However, within our range of spinel and melt compositions, the Fe^{3+}/Fe^{Total} and the Fe^{2+}/Mg^{2+} ratio of the spinel or the melt has no significant effect on V partitioning. Experiments with Cr-rich spinels show somewhat higher partitions coefficients, which is in agreement with the findings of Mallmann and O'Neill (2009). The general agreement of our data with the Mallmann and O'Neill (2009) experiments, which used different starting compositions, suggests that melt composition does not have a large effect on D_V.

To exploit the effect of fO_2 on V partition coefficients, we fitted our experimentally derived data using a nonlinear least squares routine. The fit resulted in Eq. 2, linking D_V to fO_2. We will expand on this further in the discussion section. The fit coefficients are given in Table 5.

$$\log D_V = a + b \times \log fO_2 + c \times \log fO_2{}^2 + d \times \mathrm{Cr\#(spinel)} \quad (2)$$

Copper, manganese and molybdenum

Cu, Mn, and Mo are all moderately incompatible in spinel. Copper measurements are complicated due to the fact that Cu is lost from some of the experiments. Interestingly, the amount of Cu loss is strongly dependent on oxygen fugacity, and the highest Cu loss occurs at the lowest fO_2. However, the large differences in bulk Cu concentrations do not significantly affect the partitioning, even though there is a relatively large amount of scatter of the data. The D_{Cu} values are fairly uniform, and range from 0.02 to 0.7. This implies that even though Cu is lost during some experiments, crystal melt equilibrium is (to some extent) preserved.

Mn is slightly incompatible in spinel with D values between 0.2 and 0.9. The D values are very uniform and appear to be independent of fO_2 and temperature. There seems to be a small compositional effect, with D values consistently (if only slightly) higher in Fe^{2+}-rich spinels compared to Mg-rich spinels.

Mo partitioning depends on oxygen fugacity, with D_{Mo} decreasing with increasing fO_2, from 0.085 at the lowest oxygen fugacity (log $fO_2 = -12$) to 0.0033 for the experiments performed in air (log $fO_2 = -0.7$). This could be explained by a valence state change in Mo, which may occur as Mo^{4+} or Mo^{6+} depending on the fO_2 (Holzheid et al. 1994). This suggests that the tetravalent species is more compatible, which is to be expected because it would fit better in the crystal structure than Mo^{6+}.

Similarly to V, we use a simply fitting routine to link changing fO_2 to D_{Mo}. The results of the fitting are given in Fig. 4b and Table 5.

$$\log D_{Mo} = a + b \times \log fO_2 \quad (3)$$

Titanium, scandium, the HFSE and lutetium

Ti and Sc exhibit similar partitioning behavior and are both slightly incompatible. The partition coefficients are mainly controlled by spinel composition; D_{Ti} is lowest for the Al-rich spinels (0.06–0.13), up to 0.2 for the samples containing Cr and 0.9 for sp6_08 (the Fe^{3+}-rich sample). Sc is slightly less compatible, with D_{Sc} between 0.03 and 0.14, and 0.4 for sp6_08. Furthermore, D_{Sc} values slightly decrease with increasing fO_2.

The HFSEs Nb, Ta, Zr and Hf, as well as Lu (a rare earth element), all have very similar partition coefficients. They show a similar trend to Ti, but are all about two orders of magnitude less compatible. Similar to Ti and Sc, the HFSEs are the most incompatible in the Al-rich spinels; the D values are between 10^{-4} and 10^{-3}. The spinels that contain Cr have slightly higher D values of around 10^{-3}, and for the high Fe^{3+} experiment, D_{HFSE} values are around 10^{-2}.

In particular, our D_{HFSE} values for Al-rich spinels are lower than previously published data on HFSE partitioning (Horn et al. 1994; Nielsen and Beard 2000; Nielsen et al. 1994). But as the spinel compositions in the literature are Cr^{3+} and Fe^{3+} rich (Horn et al. 1994) or Ti-magnetite rich (Nielsen and Beard, 2000; Nielsen et al., 1994), it is clear that their data follow the same trend as ours. When plotting the D values against Al cation concentration (Fig. 5a–d), our data for Al-spinels and the spinels containing some chromium or Fe^{3+} follow the same trend as the high

magnetite spinels from Nielsen et al. (1994); the Al-spinels always have the lowest D values, and the values increase strongly with both increasing Cr and increasing Fe^{3+}.

Nielsen (1994) notes that the HFSE partitioning correlates strongly with D_{Ti}. Our data suggest that both D_{Ti} and the D_{HFSE} correlate with Fe^{3+} or Cr^{3+} content, so the correlation is mainly controlled by the nature of the trivalent element in the spinel. This is likely due to a change in size of the octahedral site, both Cr and Fe^{3+} have a somewhat larger ionic radius than Al (in VI coordination: 0.645, 0.615 and 0.535 Å, respectively, Shannon 1976). The HFSE, Ti and Sc also have relatively large ionic radii. So the incorporation of Cr and Fe^{3+} appears to increase the crystal site size, which would increase the compatibility of larger elements.

It is possible that a high Ti content would affect partitioning in a similar manner, as this tetravalent element will take the same site in the crystal structure as the trivalent elements. In our experiments, however, the total Ti content is similar at 2 wt% in most experiments, while a couple of experiments have only trace amounts of Ti. There is no difference in partitioning between these experiments, suggesting that for our range of compositions, Ti has no effect.

Temperature has little effect on the partitioning. Oxygen fugacity has no direct effect on the partitioning except for Sc, but it has a large indirect effect for all these elements insofar as it changes the Fe^{3+}/total Fe ratio, and therefore, the Fe^{3+} concentration in the spinel.

Tungsten, uranium, thorium and yttrium

W, U, Th and Y are all highly incompatible in spinel, and the concentration of these elements is usually close to or below detection limit of our analytical technique. Therefore, the measured partition coefficients exhibit quite some scatter but are typically below 10^{-4}. We could not find any clear correlation between D values, temperature, fO_2 and spinel composition.

Volatile elements

The total Zn concentration in most experiments is lower than expected, with the exception of the experiments performed under the highest oxygen fugacity. This implies that Zn is significantly volatile under more reducing conditions. The D_{Zn} values for the most oxidized experiments range from 5 to 8. The elements Cd, Sn, Sb and Pb all appear to be highly volatile under all experimental conditions. In most experiments, the bulk element content is significantly

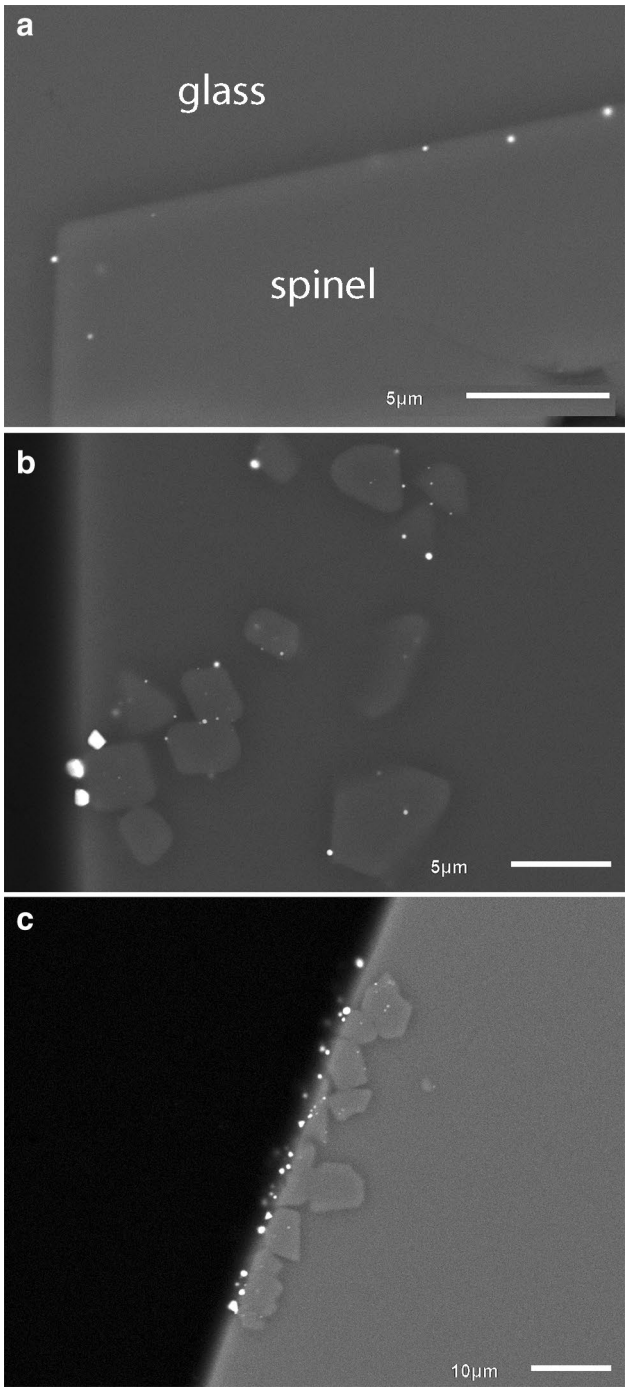

Fig. 6 Backscatter SEM images of samples that contain Pt–Rh nuggets. **a** Typical case, where the noble metal nuggets are located at the rims of the spinel crystal. Figure 6b shows the association of nuggets with small spinel crystals, at the edge of the sample. Figure 6c shows relatively large nuggets in association with small spinels, concentrated at the edge of the sample. Note that for the smaller spinel crystals, nuggets also sometimes occur inside the crystals. This is not observed for the larger spinels

decreased; therefore, meaningful partitioning coefficients for these elements could not be calculated. More experiments are clearly needed to better constrain the geochemical behavior of the moderately volatile transition metals and related elements.

Platinum group elements: platinum and rhodium

Partition coefficients

The determination of partition coefficients for PGEs is complicated due to their tendency to form metallic nanoscale particles (often termed "nano-nuggets") in silicate melts (see also the analytical procedures section). As a consequence, the PGE concentrations in melts or crystals may be overestimated at the risks of erroneous partition coefficients. This problem may explain much of the observed variation of PGE partition coefficients in the literature (Brenan et al. 2012; Capobianco and Drake 1990; Capobianco et al. 1994; Righter et al. 2004; Sattari et al. 2002).

To determine D_{Pt} and D_{Rh}, we performed two types of experiments: (1) the experiments described above, where Pt and Rh were added to the starting material together with other trace elements and (2) four additional experiments that had no trace elements added prior to the experiment (samples prg11–prg14). These experiments were equilibrated with a Pt–Rh wire loop from which the sample was suspended in the furnace. Two wires of different composition (thermocouple wire; $Pt_{70}Rh_{30}$ and $Pt_{94}Rh_6$) were used, and the experiments were performed at both relatively reducing ($\log fO_2 = -10$) and rather oxidizing ($\log fO_2 = -0.7$) conditions. This second set of experiments is designed to prevent oversaturation of Pt and Rh, which likely enhances the formation of (nano-)nuggets, and to determine whether equilibrium has been achieved by comparing the concentrations in both types of experiments. Note that the type 2 experiments were performed in an iron- and chromium-free composition.

In our experiments, the (measured) partition coefficients for Rh extend over a range of 5 orders of magnitude (see Fig. 3d). The FeO-containing samples generally have lower D values. Furthermore, D_{Rh} increases strongly with increasing oxygen fugacity, from $D_{Rh} = 1.1$ at a $\log fO_2$ of -10 to $D_{Rh} = 431$ at a $\log fO_2$ of -0.7 (for the iron-free samples).

Partition coefficients for Pt are not affected by fO_2, but similar to Rh, the iron-containing experiments have lower D values (see Table 4). For both Pt and Rh, the type 1 experiments give similar results to the type 2 experiments. The composition of the wire loop also has very little effect

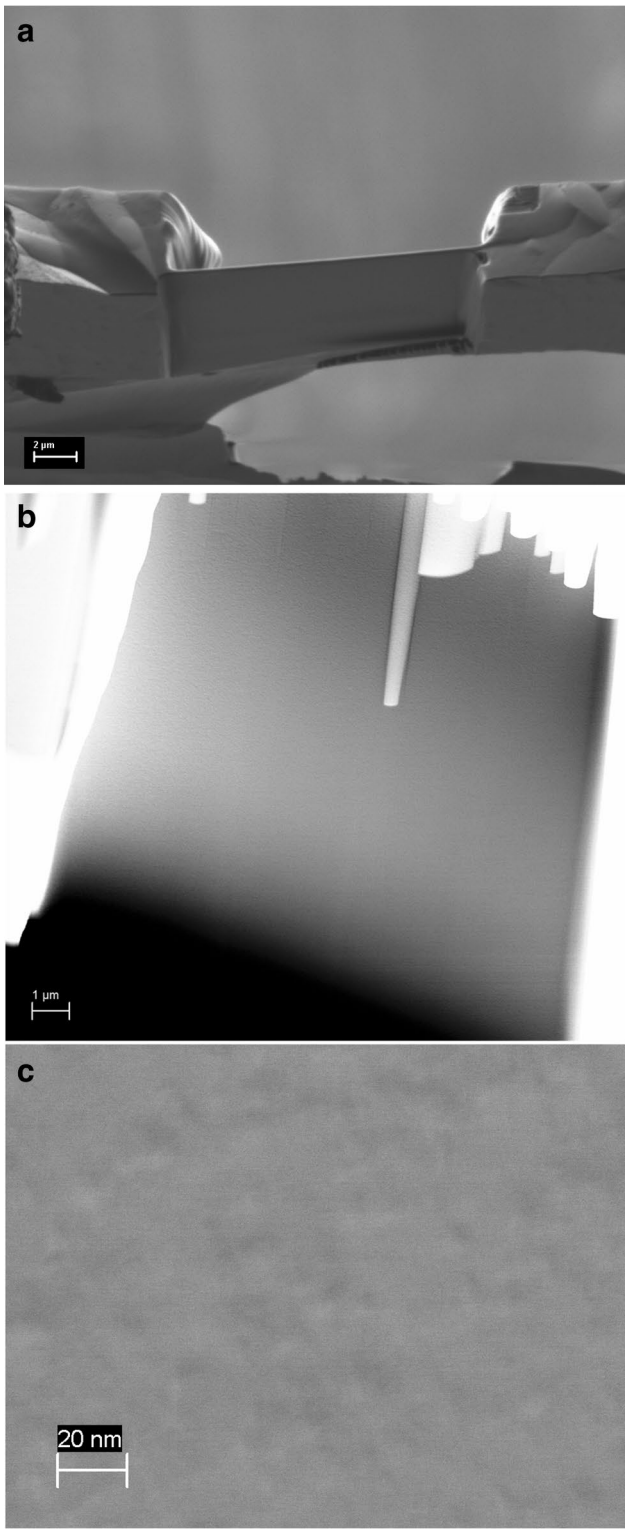

Fig. 7 **a** Lamellae of a spinel crystal prepared for TEM analysis. **b**, **c** STEM-HAADF images from sample sp2_10, where no obvious high-Z nano-nuggets are detected

on the amount of Pt and Rh in the experiment, and the Pt/Rh ratio. There is a, however, a certain amount of scatter in the data which could be the result of either analytical uncertainties or contamination of the measurements by nuggets.

The issue of (nano)nuggets

Overall, the measured Pt concentrations of the glasses of all experiments is similar within one order of magnitude independent of fO_2. This is not what we expected when considering that the solubility of Pt and Rh in silicate melts increases with increasing fO_2 (Ertel et al. 1999). The Rh content shows a bit more scatter. This is in part due to varying amounts of Rh in the experiments, because some experiments were performed with a 100 % Pt wire loop, while others were performed with a Rh-containing wire loop. However, despite the scatter, there seems to be a slight increase in Rh with increasing fO_2. According to Ertel et al. (1999), both Pt and Rh concentrations in glass should decrease strongly with decreasing fO_2, but our data does not show this. At lower fO_2 (<log −6), the measured Pt and Rh concentrations in the melt are much higher than that predicted by the solubility model. This suggests that if the Ertel et al. (1999) model is correct, under low fO_2 conditions, Pt and Rh are for the most part not dissolved in the melt but present as metallic nuggets. At first sight, this seems to discredit our measured Pt and Rh partition coefficients derived from the low fO_2 experiments.

However, our data show clearly that the change in apparent D_{Rh} values in our experiments is almost entirely due to changes of the Rh content in the spinel (Table 4), which is low at low fO_2 and increases dramatically with increasing fO_2 (up to ~ 4700 ppm Rh). In contrast, the Pt concentration in spinel is rather constant with fO_2 and is only lower in the Fe-bearing experiments. However, the experiments at high fO_2 show the least amount of scatter in concentrations and D values, suggesting that nuggets are indeed less of an issue under these conditions. It is conceivable that at low fO_2 conditions, both the Pt and Rh concentrations in the glass are overestimated due to the presence of metallic nuggets, and the partition coefficients could therefore be underestimated. This could mean that the decreasing D values for Rh with decreasing fO_2 are at least partly artificial and caused by nugget contamination; however, it is unclear why this is not also the case for Pt.

Occurrence and concentration of nuggets

All samples were carefully examined by high-resolution SEM imaging for Pt–Rh nuggets, to avoid contamination of the LA-ICP-MS measurements. In some experiments, we do indeed find Pt–Rh alloy nuggets of submicron size. These nuggets occur on the rims of the spinels. We did not observe any metallic nuggets in the cores of large (>20 μm) spinels. Therefore, we do not expect the nuggets to interfere with the LA-ICP-MS measurements because the rims of the crystals are easily avoided during measurements.

The occurrence of platinum nuggets at the rims of spinels in experiments was also observed by Ballhaus et al. (2006); Brenan et al. (2012); Finnigan et al. (2008). Ballhaus et al. (2006) suggests that this might be due to preferable nucleation of the nuggets on the (Cr)-spinel surface. Finnigan et al. (2008) propose that local reduction at the crystal–melt interface caused by preferred uptake of oxidized species of Fe (Fe^{3+} over Fe^{2+}) and Cr (Cr^{3+} over Cr^{2+}) in spinel could result in a decreased solubility of PGEs at this interface, which results in the precipitation of nuggets. However, the fact that the nuggets occur in all types of experiments, including the ones that are Fe and Cr free, suggests that local reduction does not play a role in these cases. Furthermore, the association of relatively large nuggets with very small spinel crystals in one sample (sp10_02) suggests that local reduction in the melt due to the formation of these small crystals would not be sufficient to allow such relatively large amount of Pt–Rh alloy to precipitate.

To investigate the occurrence and nature of these nuggets further, two samples were examined in more detail. Both samples are type 1 experiments, i.e. trace elements (including Pt and Rh) were added to the starting material, and they are also equilibrated with a $Pt_{94}Rh_6$ wire loop during the run. Sample 10_02 was performed at relatively oxidizing conditions ($\log fO_2 = -4$) and high temperature (1420 °C). The sample contains relatively large nuggets (see Fig. 6b, c), up to nearly one micron in diameter, which is large enough for EDS analysis. The largest nuggets are always found in association with smaller spinel crystals, typically occurring at the edge of the sample, but not necessarily close to the wire loop. Smaller nuggets are also observed on the rims of larger spinels in the sample (Fig. 6a). An EDS spectrum from these nuggets suggests that the Pt/Rh ratio is approximately 1.1. This is, considering the uncertainties, very similar to the measured Pt/Rh ratio in the melt of 1.3, which suggests that either the nuggets have precipitated from this melt without any significant fractionation of Pt from Rh or that the measurements of the glass are dominated by nano-nuggets of a similar composition to the larger ones.

To search for nano-nuggets inside spinel, we characterized a spinel crystal of one sample (sp2_10) using TEM (see Fig. 7a–c). These spinels contained particularly high Rh (~ 1000 ppm) and moderately high Pt concentrations (10 ppm). However, no nuggets were found inside the spinel on various STEM-HAADF images throughout the prepared lamella although the spatial resolution was

sufficiently high to identify possible nuggets in the size range < 10 nm (Fig. 7b, c). This experiment was performed under high fO_2 (log −0.7), indicating that under these oxidizing conditions, the concentrations of Pt and Rh in the spinel structure is indeed rather high. This confirms in part the finding of Righter and Downs (2001), who have shown that under highly oxidizing conditions, magnesioferrite ($Mg(Fe^{3+})_2O_4$) can accommodate large amounts of PGEs in the crystal structure. In natural systems Park et al. (2012) found high Rh and other PGE contents in natural Cr spinels from oxidized lavas.

Under oxidizing conditions, the solubility of Pt and Rh in the melt is also rather high, which suggests that at least for the high fO_2 experiments, there is no reason to believe that the measurements are contaminated by nuggets either in the spinels or the melt and that the partition coefficients for the high fO_2 experiments are reliable. However, further TEM investigations on more lamellae are needed to fully address the problem of the possible presence of nano-nuggets.

Some comments on Pt and Rh transport in silicate melts

Although our experiments were primarily designed to measure partition coefficients, we can use the experiments to shed some additional light on PGE transport processes in silicate melts. Despite the fact that solubility of Pt and Rh is very low, especially at low oxygen fugacities, the mobility of these elements is high enough to allow transport of enough material to allow the formation of metallic nuggets at the rims of crystals. Our type 2 experiments contained no Pt or Rh in the starting material (see Table 4 and section "Partition coefficients"). The Pt and Rh content in these experiments is entirely derived from the metal wire loop, which holds the sample in the furnace. Depending on redox conditions, the spinels growing in these experiments contained significant to very high Pt and Rh concentrations after the run. The Pt and Rh in these experiments had to be chemically dissolved, or in some other way physically transported from the metal wire loop. The concentrations of Pt and Rh in the glass and spinel are always very similar to those of the experiments that have Pt and Rh added before the experiment (type 1 experiments). This suggests that some sort of equilibrium situation has been reached, despite the fact that in the reducing experiments, the measurements of the glasses may be dominated by nuggets.

The composition of the wire has very little effect on the concentration measured in the glasses or the spinels. The Pt/Rh ratio, however, is very different from that of the platinum wire loop from which the experiments equilibrated (Pt/Rh of the wire is 15.7 or 2.3 depending on the wire). The low fO_2 experiments give a Pt/Rh ratio of ~ 20 in both spinel and melt, while the high fO_2 have a Pt/Rh ratio of 0.6 in the melt and 0.02 in the spinels. This is an important observation, because it means that, even if the measurement of the low fO_2 experiments are dominated by nuggets, these metallic nuggets are not simply flakes of Pt–Rh wire material that have been dispersed into the melt. Instead, significant fractionation occurs when Pt and Rh are transported from the wire through the melt and to the crystals, and, in the case of the high fO_2 experiments, also when the spinels crystalize from the melt. It should also be noted that the fractionation of Pt from Rh occurs into different directions under different oxygen fugacities; at low fO_2, Pt/Rh increases, while at high fO_2, it is the other way around, Pt/Rh decreases. This indicates that Pt can be significantly fractionated from Rh during melt transport in silicate melts and that this fractionation depends critically on fO_2.

Implications and applications

Oxygen geobarometry using redox-sensitive trace elements

Our experimentally determined partition coefficients may be used to predict trace element evolution of spinel from fractionating mafic magmas. The most straightforward case in which one could use our data to predict the redox conditions during spinel growth involves spinel-hosted melt inclusions. In this case, one would need to measure both the host spinel and the melt inclusions for Mo or V, calculate D_{Mo} or D_V from the spinel/melt inclusion data, and use the aforementioned equations (2, 3) which links D_{Mo} or D_V to fO_2.

If no melt inclusions are available, the determination of fO_2 is more complicated. One could, however, use relative redox indicators such as Mo/Ga or V/Ni ratios in spinels to establish whether spinels were formed at relatively more oxidizing or more reducing conditions. As an example, consider a spinel which was formed early during fractionation from a near-primary basaltic magma, compared to a spinel which was formed (or re-equilibrated) later during contact with an evolved (and more oxidized) magma in a magma reservoir. The first spinel is probably a Cr-rich spinel (Barnes and Roeder 2001) that formed under relatively reducing conditions. As Mo or V are more compatible under these conditions, the spinel is expected to show a relatively high Mo/Ga and V/Ni ratio. Note that Ga and Ni partition coefficients are relatively constant and are not significantly affected by changing melt composition, crystal composition or fO_2.

The spinel that formed later during the crystallization sequence crystallizes under more oxidizing conditions, where Mo and V are much more incompatible. Here, the Mo/Ga and V/Ni should be much lower than in the reducing

case. This approach will work only well when the system is not disturbed by the crystallization of other silicate or oxide phases. Both the Ga and Ni bulk partitioning coefficients during mantle melting are not far from 1 (Davis et al. 2013), so there is some potential that our proposed trace element ratios may be used as a relative redox indicator, but this needs to be tested further. In the case of basalts, the V/Sc ratio is often used in a similar way to constrain variations in fO_2 (Lee et al. 2005; Mallmann and O'Neill 2009); however, in case of spinel solid solutions, this is not recommended since D_{Sc} highly depends on the spinel major element composition, i.e. the Cr#, and the Fe^{3+} content, and the latter is controlled by the redox conditions.

Conclusions

We determined spinel/melt partition coefficients for a number of trace elements, as a function of spinel composition and oxygen fugacity conditions. For many trace elements, there is little or no effect of either composition or fO_2 on the partitioning behavior. However, partition coefficients of the multivalent elements V and Mo are dependent of redox conditions. These elements may be used to constrain relative oxygen fugacity during spinel formation or re-equilibration.

For Ti, the HFSE, Sc and Lu (representing the rare earth elements), the spinel composition is the major controlling factor of their partitioning.

The partitioning of Pt and Rh is more complicated due to the issue of metallic nuggets in the melt. We find strong effects of fO_2 on the partitioning of Rh, while Pt appears unaffected by oxygen fugacity. At high fO_2, nuggets are not an issue, and we find high D values for Rh. We also report that a fractionation of Pt from Rh can occur during melt transport in silicate melts and that the direction of this fractionation depends on fO_2: at low fO_2 the Pt/Rh increases, while at higher fO_2, Pt/Rh decreases.

Acknowledgments Our thanks go to the workshops at the Mineralogical Institute at Münster University and especially to Maik Trogisch for help with the sample preparation. Furthermore, we would like to thank Martina Menneken and Joachim Krause for their assistance with the LA-ICP-MS measurements, and Arno Rohrbach for support in the lab. Kristina Dunkel and Moritz Barth are thanked for TEM sample preparation. We thank Roger Nielsen and Kevin Righter for their constructive reviews that helped improve this paper, and Mark Ghiorso for the editorial handling.

References

Aigner-Torres M, Blundy J, Ulmer P, Pettke T (2007) Laser Ablation ICPMS study of trace element partitioning between plagioclase and basaltic melts: an experimental approach. Contrib Mineral Petrol 153:647–667

Arai S (1992) Chemistry of chromian spinel in volcanic-rocks as a potential guide to magma chemistry. Mineral Mag 56:173–184

Ballhaus C, Sylvester P (2000) Noble metal enrichment processes in the Merensky Reef, Bushveld Complex. J Petrol 41:545–561

Ballhaus C, Bockrath C, Wohlgemuth-Ueberwasser C, Laurenz V, Berndt J (2006) Fractionation of the noble metals by physical processes. Contrib Mineral Petrol 152:667–684

Barnes SJ, Roeder PL (2001) The range of spinel compositions in terrestrial mafic and ultramafic rocks. J Petrol 42:2279–2302

Beattie P (1994) Systematics and energetics of trace-element partitioning between olivine and silicate melts—implications for the nature of mineral melt partitioning. Chem Geol 117:57–71

Berry AJ, O'Neill HSC (2004) A XANES determination of the oxidation state of chromium in silicate glasses. Am Mineral 89:790–798

Blundy J, Wood B (1994) Prediction of crystal-melt partition-coefficients from elastic-moduli. Nature 372:452–454

Blundy J, Wood B (2003) Partitioning of trace elements between crystals and melts. Earth Planet Sci Lett 210:383–397

Brenan JM, Finnigan CF, McDonough WF, Homolova V (2012) Experimental constraints on the partitioning of Ru, Rh, Ir, Pt and Pd between chromite and silicate melt: the importance of ferric iron. Chem Geol 302:16–32

Canil D (1999) Vanadium partitioning between orthopyroxene, spinel and silicate melt and the redox states of mantle source regions for primary magmas. Geochim Cosmochim Acta 63:557–572

Capobianco CJ, Drake MJ (1990) Partitioning of ruthenium, rhodium, and palladium between spinel and silicate melt and implications for platinum group element fractionation trends. Geochim Cosmochim Acta 54:869–874

Capobianco CJ, Hervig RL, Drake MJ (1994) Experiments on crystal liquid partitioning of Ru, Rh and Pd for magnetite and hematite solid-solutions crystallized from silicate melt. Chem Geol 113:23–43

Davis FA, Humayun M, Hirschmann MM, Cooper RS (2013) Experimentally determined mineral/melt partitioning of first-row transition elements (FRTE) during partial melting of peridotite at 3 GPa. Geochim Cosmochim Acta 104:232–260

Deines P, Nafziger RH, Ulmer GC, Woermann E (1976) Temperature-oxygen fugacity tables for selected gas-mixtures in system C–H–O at one atmosphere total pressure. Metall Trans B 7:143

Dick HJB, Bullen T (1984) Chromian spinel as a petrogenetic indicator in abyssal and alpine-type peridotites and spatially associated lavas. Contrib Mineral Petrol 86:54–76

Ertel W, O'Neill HS, Sylvester PJ, Dingwell DB (1999) Solubilities of Pt and Rh in a haplobasaltic silicate melt at 1300 degrees C. Geochim Cosmochim Acta 63:2439–2449

Finnigan CS, Brenan JM, Mungall JE, McDonough WF (2008) Experiments and models bearing on the role of chromite as a collector of platinum group minerals by local reduction. J Petrol 49:1647–1665

Fortenfant SS, Gunther D, Dingwell DB, Rubie DC (2003) Temperature dependence of Pt and Rh solubilities in a haplobasaltic melt. Geochim Cosmochim Acta 67:123–131

Ganguly J, Ito M, Zhang XY (2007) Cr diffusion in orthopyroxene: experimental determination, Mn-53-Cr-53 thermochronology, and planetary applications. Geochim Cosmochim Acta 71:3915–3925

Hill R, Roeder P (1974) Crystallization of spinel from basaltic liquid as a function of oxygen fugacity. J Geol 82:709–729

Holzheid A, Borisov A, Palme H (1994) The effect of oxygen fugacity and temperature on solubilities of nickel, cobalt, and molybdenum in silicate melts. Geochim Cosmochim Acta 58:1975–1981

Horn I, Foley SF, Jackson SE, Jenner GA (1994) Experimentally determined partitioning of high-field strength-elements and selected transition-elements between spinel and basaltic melt. Chem Geol 117:193–218

Jackson SE (2001) The application of Nd:YAG lasers in LA-ICP-MS. Principles and applications of laser ablation-mass spectrometry in the earth. In: Mineralogical Association of Canada Short Course Series, vol 29, pp 29–46

Jochum KP, Willbold M, Raczek I, Stoll B, Herwig K (2005) Chemical characterisation of the USGS reference glasses GSA-1G, GSC-1G, GSD-1G, GSE-1G, BCR-2G, BHVO-2G and BIR-1G using EPMA, ID-TIMS, ID-ICP-MS and LA-ICP-MS. Geostand Geoanal Res 29:285–302

Jochum KP et al (2011) Determination of reference values for NIST SRM 610-617 Glasses following ISO guidelines. Geostand Geoanal Res 35:397–429

Lee CTA, Leeman WP, Canil D, Li ZXA (2005) Similar V/Sc systematics in MORB and arc basalts: implications for the oxygen fugacities of their mantle source regions. J Petrol 46:2313–2336

Mallmann G, O'Neill HSC (2009) The crystal/melt partitioning of v during mantle melting as a function of oxygen fugacity compared with some other elements (Al, P, Ca, Sc, Ti, Cr, Fe, Ga, Y, Zr and Nb). J Petrol 50:1765–1794

Mallmann G, O'Neill HS (2013) Calibration of an empirical thermometer and oxybarometer based on the partitioning of Sc, Y and V between olivine and silicate melt. J Petrol 54:933–949

Naldrett AJ, Wilson A, Kinnaird J, Chunnett G (2009) PGE tenor and metal ratios within and below the merensky reef, bushveld complex: implications for its genesis. J Petrol 50:625–659

Nielsen RL, Beard JS (2000) Magnetite-melt HFSE partitioning. Chem Geol 164:21–34

Nielsen RL, Gallahan WE, Newberger F (1992) Experimentally determined mineral-melt partition-coefficients for Sc, Y and Ree for olivine, ortho-pyroxene, pigeonite, magnetite and ilmenite. Contrib Mineral Petrol 110:488–499

Nielsen RL, Forsythe LM, Gallahan WE, Fisk MR (1994) Major-element and trace-element magnetite-melt equilibria. Chem Geol 117:167–191

Page P, Barnes SJ (2009) Using trace elements in chromites to constrain the origin of podiform chromitites in the Thetford mines ophiolite, Quebec, Canada. Econ Geol 104:997–1018

Park JW, Campbell IH, Eggins SM (2012) Enrichment of Rh, Ru, Ir and Os in Cr spinels from oxidized magmas: evidence from the Ambae volcano, Vanuatu. Geochim Cosmochim Acta 78:28–50

Righter K, Downs RT (2001) The crystal structures of synthetic Re- and PGE-bearing magnesioferrite spinels: implications for impacts, accretion and the mantle. Geophys Res Lett 28(4):619–622

Righter K, Campbell AJ, Humayun M, Hervig RL (2004) Partitioning of Ru, Rh, Pd, Re, Ir, and Au between Cr-bearing spinel, olivine, pyroxene and silicate melts. Geochim Cosmochim Acta 68:867–880

Righter K, Leeman WP, Hervig RL (2006) Partitioning of Ni, Co and V between spinel-structured oxides and silicate melts: importance of spinel composition. Chem Geol 227:1–25

Roeder PL, Reynolds I (1991) Crystallization of chromite and chromium solubility in basaltic melts. J Petrol 32:909–934

Sattari P, Brenan JM, Horn I, McDonough WF (2002) Experimental constraints on the sulfide- and chromite–silicate melt partitioning behavior of rhenium and platinum-group elements. Econ Geol Bull Soc 97:385–398

Shannon RD (1976) Revised effective ionic-radii and systematic studies of interatomic distances in halides and chalcogenides. Acta Crystallogr Sect A 32(Sep1):751–767

Toplis MJ, Corgne A (2002) An experimental study of element partitioning between magnetite, clinopyroxene and iron-bearing silicate liquids with particular emphasis on vanadium. Contrib Mineral Petrol 144:22–37

van Westrenen W, Draper DS (2007) Quantifying garnet-melt trace element partitioning using lattice-strain theory: new crystal-chemical and thermodynamic constraints. Contrib Mineral Petrol 154:717–730

Yang H, Salmon JF, Foster WR (1972) Phase equilibria of join akermanite–anorthite–forsterite in system CaO–MgO–Al_2O_3–SiO_2 at atmospheric-pressure. Am J Sci 272:161